1×10^6 cells/mL, incubated for 20 min with a fluorescein isothiocyanate (FITC)-conjugated antibody against CD49b or CD98 (BioLegend) or a phycoerythrin (PE)-conjugated antibody against CD10, CD13, CD29, CD44, CD49a, CD49c, CD49d, CD49e, CD51/61, CD73, CD90, CD105, CD117, SSEA4, HLA-A,B,C (BioLegend), CD133/1 (Miltenyi Biotec), or CD166 (Beckman Coulter). Nonspecific staining was assessed using relevant isotype controls. Dead cells were excluded using the Live/Dead Fixable Far Red Dead Cell Stain Kit (Life Technologies). FlowJo software was used for quantitative analysis.

RNA extraction, cDNA generation, and quantitative polymerase chain reaction

Total RNA was extracted using the RNeasy Mini Kit (Qiagen) accroding to the manufacturer's instructions. cDNA was generated from 1 μg of total RNA using the Verso cDNA Synthesis Kit (Thermo Scientific) and purified using the MinElute PCR Purification Kit (Qiagen). Quantitative polymerase chain reaction (Q-PCR) analysis was conducted using the SsoFast EvaGreen supermix (Bio-Rad) according to the manufacturer's protocols. The relative expression value for each gene was calculated using the ΔΔCt method, and the most reliable internal control gene was determined using geNorm Software (http://medgen.ugent.be/~jvdesomp/genorm/). Details of the primers used in these experiments are available on request.

Western blot analysis

Whole cell extracts were prepared by washing cells with ice-cold PBS and lysing them with M-PER Mammalian Protein Extraction Reagent (Thermo Scientific Pierce) according to the manufacturer's instructions. Nuclear and cytosolic extracts were prepared as follows. Cells were washed with ice-cold PBS and lysed with lysis buffer (50 mM Tris-HCl (pH 7.5), 0.5% Triton X-100, 137.5 mM NaCl, 10% glycerol, 5 mM EDTA, 1 mM sodium vanadate, 50 mM sodium fluoride, 10 mM sodium pyrophosphate, and protease inhibitor cocktail). Then, insoluble nuclei were isolated by centrifugation and lysed with lysis buffer containing 0.5% SDS. Equal amounts of proteins were separated by sodium dodecyl sulfate polyacrylamide gel electrophoresis (SDS-PAGE), transferred to polyvinylidene fluoride membranes (Immobilon-P; Millipore), and probed with antibodies against cleaved Notch1 (#2421; Cell Signaling Technology), HIF-1α (#610959; BD Bioscience), hypoxia-inducible factor 2α (MAB3472; Millipore), Akt (#9272; Cell Signaling Technology), and phospho Akt (Ser473) (#4060; Cell Signaling Technology). Horseradish peroxidase (HRP)-conjugated anti-mouse or -rabbit IgG antibody (Cell Signaling Technology) was used as a secondary antibody, and immunoreactive bands were visualized using Immobilon Western Chemiluminescent HRP substrate (Millipore). The band intensity was measured using the ImageJ software.

Fluorescence microscopy

Phase-contrast and fluorescence images were obtained using a fluorescence microscope (BZ-9000; Keyence) using BZ Analyzer Software (Keyence).

Adipogenic, osteogenic, and chondrogenic differentiation procedures

For adipogenic differentiation, cells were cultured in differentiation medium (Zen-Bio). After 7 days, half of the medium was exchanged for adipocyte medium (Zen-Bio) and this was repeated every 3 days. Three weeks after differentiation, adipogenic differentiation was confirmed by a microscopic observation of intracellular lipid droplets with the aid of Oil Red O staining. Osteogenic differentiation was induced by culturing the cells in osteocyte differentiation medium (Zen-Bio). Differentiation was examined by Alizarin Red staining. For chondrogenic differentiation, 2×10^5 hADMSCs were centrifuged at 400 g for 10 min. The resulting pellets were cultured in chondrogenic medium (Lonza) for 21 days. The pellets were fixed with 4% paraformaldehyde in PBS, embedded in OCT, frozen, and sectioned at 8 μm. The sections were incubated with PBSMT (PBS containing 0.1% Triton X-100, and 2% skim milk) for 1 h at room temperature, and then incubated with a mouse monoclonal antibody against type II collagen (Abcam) for 1 h. After washing with PBS, cells were incubated with Alexa 546-conjugated anti-mouse IgG to identify chondrocytes (Life Technologies). The cells were counterstained with 4'-6-diamidino-2-phenylindole (DAPI) (Life Technologies) to identify cellular nuclei. The sections were also stained with 1% alcian blue (Sigma Aldrich) in 3% acetic acid, pH 2.5 for 30 min.

Determination of HK, PFK, LDH, PDH, and Cox IV activities

Cells (2×10^6) were lysed, and HK, PFK, LDH, or PDH activity was measured using the Hexokinase Colorimetric Activity Kit, Phosphofructokinase (PFK) Activity Colorimetric Assay Kit, Lactate Dehydrogenase (LDH) Activity Assay Kit, or Pyruvate Dehydrogenase Activity Colorimetric Assay Kit (all from BioVision), respectively, according to the manufacturer's instructions. To measure Cox IV activity, mitochondria were isolated from 2×10^7 cells using a Mitochondria Isolation Kit (Thermo Scientific) and lysed with buffer containing n-Dodecyl β-D-maltoside, followed by measurement with the Mitochondria Activity Assay (Cytochrome C Oxidase Activity Assay) Kit (BioChain Institute), according to the manufacturer's instructions.

Results

5% oxygen hypoxic culture condition increases proliferation capacity and decreases senescence

hADMPCs were cultured under 20% oxygen (normoxia; Nx) or 5% oxygen (hypoxia; Hx), and their proliferation capacities were examined based on the relationship between the number of cultivation days and the population doubling level (PDL). Nx-cultured hADMPCs ceased proliferation at a PDL of 35–40 (between 46–70 days), whereas continuous cell proliferation beyond 45 PDL was observed when hADMPCs were cultured in the Hx condition (Fig. 1A). To investigate whether this increase of PDL in the Hx culture condition resulted from an increase in cell cycle progression and increase in survival rates, EdU, an alternative to 5-bromo-2'-deoxyuridine (BrdU), was incorporated into the
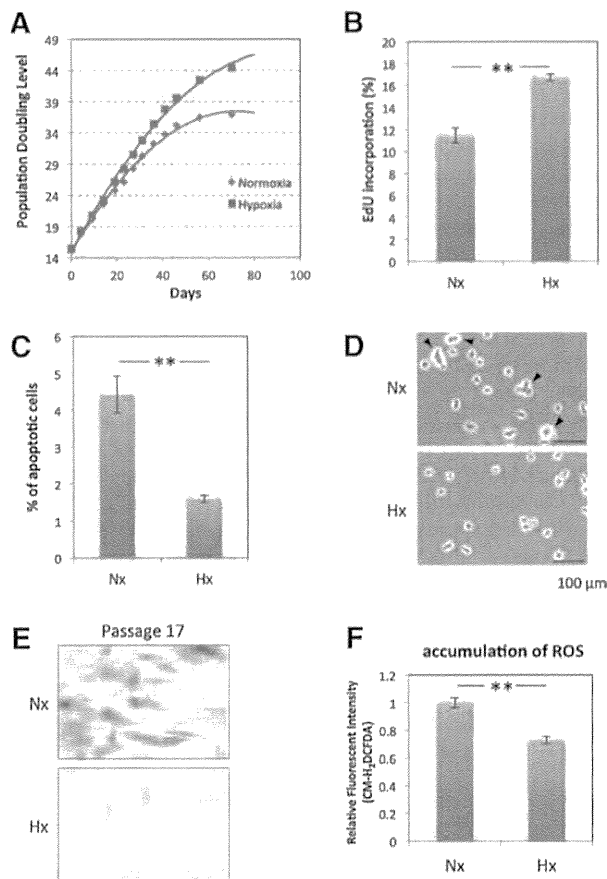
A

B

C

D

E

F

FIG. 1. Hypoxia increases proliferation capacity and decreases senescence in tissue-derived multilineage progenitor cells (hADMPCs). **(A)** Growth profiles of hADMPCs under normoxic (*red square*) and hypoxic (*blue square*) conditions. The population doubling level (PDL) was determined to be 0 when cells were isolated from human adipose tissue. Cells were maintained until they reached PDL13–15 (passage 3) and then split into four aliquots of equal cell densities. PDL was calculated based on the total cell number at each passage. **(B)** Detection of normoxic (Nx) and hypoxic (Hx) cells by flow cytometry after incorporation of EdU. **(C)** Percentages of apoptotic cells with sub-G1 DNA under Nx and Hx conditions. The results are presented as the mean of three independent experiments. **(D)** hADMPCs cultured under Nx and Hx conditions were harvested by trypsin-EDTA and then imaged using a phase-contrast microscope. *Arrowheads* indicate cells with a larger and more irregular shape. **(E)** Cells expanded under Nx and Hx conditions were stained with SA-β-gal. **(F)** Cellular reactive oxygen species detection by the oxidative stress indicator CM-H$_2$DCFDA in hADMPCs under Nx or Hx. Data are presented as the mean fluorescence intensity of three independent experiments. Error bars indicate SD. **$P < 0.01$ indicates significant difference (independent t-test) between Nx and Hx. Scale bars; 100 μm. Color images available online at www.liebertpub.com/scd

genomic DNA of the hADMPCs, and the amount of incorporated EdU was quantified by flow cytometry. As shown in Fig. 1B, the EdU incorporation rate was significantly higher in Hx-cultured hADMPCs than in Nx-cultured hADMPCs, suggesting that cell growth was increased in the Hx culture condition. In addition, measurement of DNA content in hADMPCs revealed a slight but significant decrease of sub-G1 peaks, which indicates the existence of apoptotic cells with degraded DNA, when the cells were cultured in the Hx condition (Fig. 1C). These data suggest that the Hx culture condition increases the proliferation capacity of hADMPCs by promoting their cell growth and survival rates. We also found that Nx-cultured hADMPCs were larger with a more irregular shape (Fig. 1D), which suggests that the Hx culture condition prevented hADMPCs from entering senescence [35]. To further investigate this phenomenon, cellular senescence was measured by staining for SA-β-Gal, which revealed that SA-β-Gal activity was increased in Nx-cultured hADMPCs at passage 17 (Fig. 1E). Since it has been hypothesized that senescence results from oxidative stress [20], accumulation of ROS in hADMPCs was detected using the nonfluorescent probe, CM-H$_2$DCFDA. Flow cytometry analysis revealed that ROS were generated at higher levels in hADMPCs when cultured in the Nx condition (Fig. 1F), suggesting that reduced production of ROS in the Hx condition may prevent the cells from entering replicative senescence.

Hypoxic culture maintains some MSC properties and increases differentiation

We then examined the cell properties of hADMPCs under Nx and Hx conditions. Initially, cell surface antigens expressed on hADMPCs were analyzed by flow cytometry. No significant difference in expression profile between hADMPCs cultured in Nx and Hx was observed; the cells were consistently positive for CD10, CD13, CD29, CD44, CD49a, CD49b, CD49c, CD49d, CD49e, CD51/61, CD54, CD59, CD73, CD90, CD98, CD105, CD166, and HLA-A, B, C, but negative for CD34, CD45, CD117, and CD133 (Fig. 2 and data not shown). These data were consistent with previous reports describing the expression profiles of cell surface markers of hMSCs [36,37]. To further examine the stem cell properties of hADMPCs, their potential for differentiation into adipocyte, osteocyte, and chondrocyte lineages was analyzed at passage 8. Hx-cultured hADMPCs presented enhanced differentiation into various lineages (Fig. 3A, B), indicating that the Hx culture condition improved the stem cell properties of hADMPCs.

Hypoxic culture condition activates Notch signaling

To reveal the molecular mechanism by which the Hx culture condition increased the proliferative capacity and maintained the stem cell properties of hADMPCs, we next examined Notch signaling, which is required for maintaining stem-cell features of various types of stem cells [30,31]. As expected, levels of cleaved NOTCH1, an activated form of NOTCH1, were significantly increased (greater than twofold) in the Hx culture condition (Fig. 4A). Q-PCR analysis revealed that HES1, a downstream target of Notch signaling, was upregulated in Hx-cultured hADMPCs, which also indicated that Notch signaling was activated in
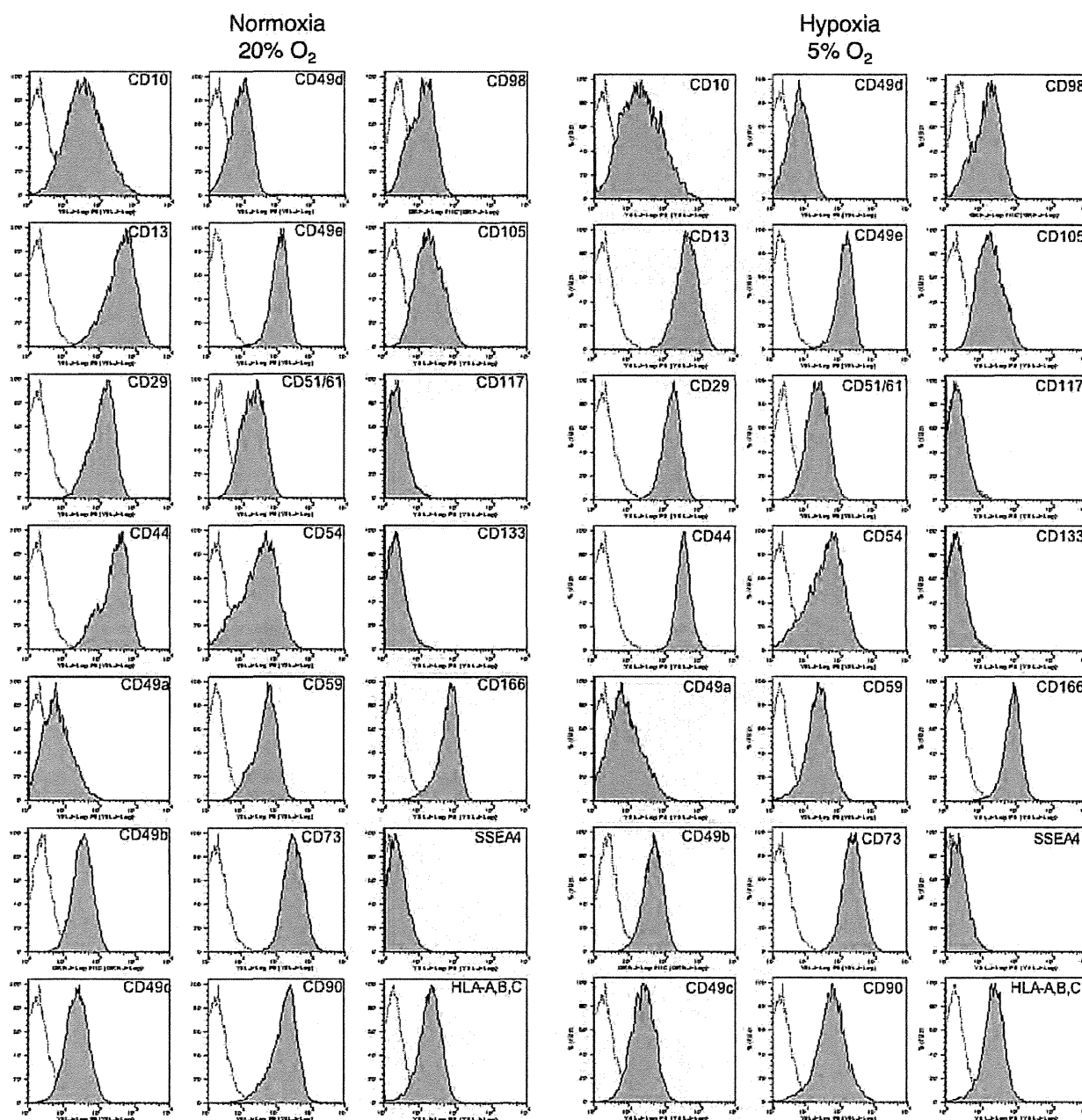
Normoxia
20% O$_2$

Hypoxia
5% O$_2$

FIG. 2. Hypoxic culture maintains mesenchymal stem cell properties. hADMPCs cultured under normoxia (20% O$_2$) or hypoxia (5% O$_2$) were labeled with antibodies against the indicated antigens and analyzed by flow cytometry. Representative histograms are shown. The respective isotype control is shown as a *gray line*.

the Hx culture condition (Fig. 4B). Administration of the γ-secretase inhibitor DAPT at 1 μM, which was sufficient to inhibit the proteolytic cleavage of NOTCH1 (Fig. 4A), decreased the Hx-induced expression of HES1 at both mRNA and protein levels (Fig. 4B, C). These data indicate that Hx increased the expression of HES1 through activation of Notch signaling. It has been reported that Notch signaling and hypoxia-inducible factor (HIF) undergo crosstalk in hypoxic cells [38–41]. Therefore, HIF-1α and HIF-2α protein levels in hADMPCs were analyzed by western blotting.

HIF-1α was stabilized when a chemical hypoxia-mimicking agent, cobalt chloride, was applied in the culture; whereas no obvious increase of HIF-1α was observed in the Hx culture condition (Fig. 4D). However, we did not detect any HIF-2α expression even in the presence of cobalt chloride (Fig. 4E). Q-PCR analysis revealed that *HIF2A* mRNA was not expressed in these cells (data not shown). From these results, we concluded that neither HIF-1α nor HIF-2α was involved in the Hx-induced increase in the proliferative capacity and stem cell properties of hADMPCs.

A

FIG. 3. Hypoxic culture enhances stem cell properties. hADMPCs were expanded under normoxic and hypoxic conditions. (A) Normoxic (20% O_2) and hypoxic (5% O_2) cells at passage 8 were induced for 3 weeks to differentiate into osteoblasts and adipocytes and stained with Alizarin Red and Oil-Red O, respectively. The stained dye was extracted, and OD values were measured and plotted as the means of three independent experiments ± SD. *$P < 0.05$. Scale bars, 200 μm. (B) Normoxic (20% O_2) and hypoxic (5% O_2) cells at passage 8 were induced for 3 weeks to differentiate to chondrocytes, and immunofluorescent analysis of collagen II (*red*) and Alucian Blue staining were performed. The *blue* signals indicate nuclear staining. Scale bars, 100 μm. Noninduced control cultures in growth medium without adipogenic, osteogenic or chondrogenic differentiation stimuli are shown (Undifferentiated). Color images available online at www.liebertpub.com/scd

B
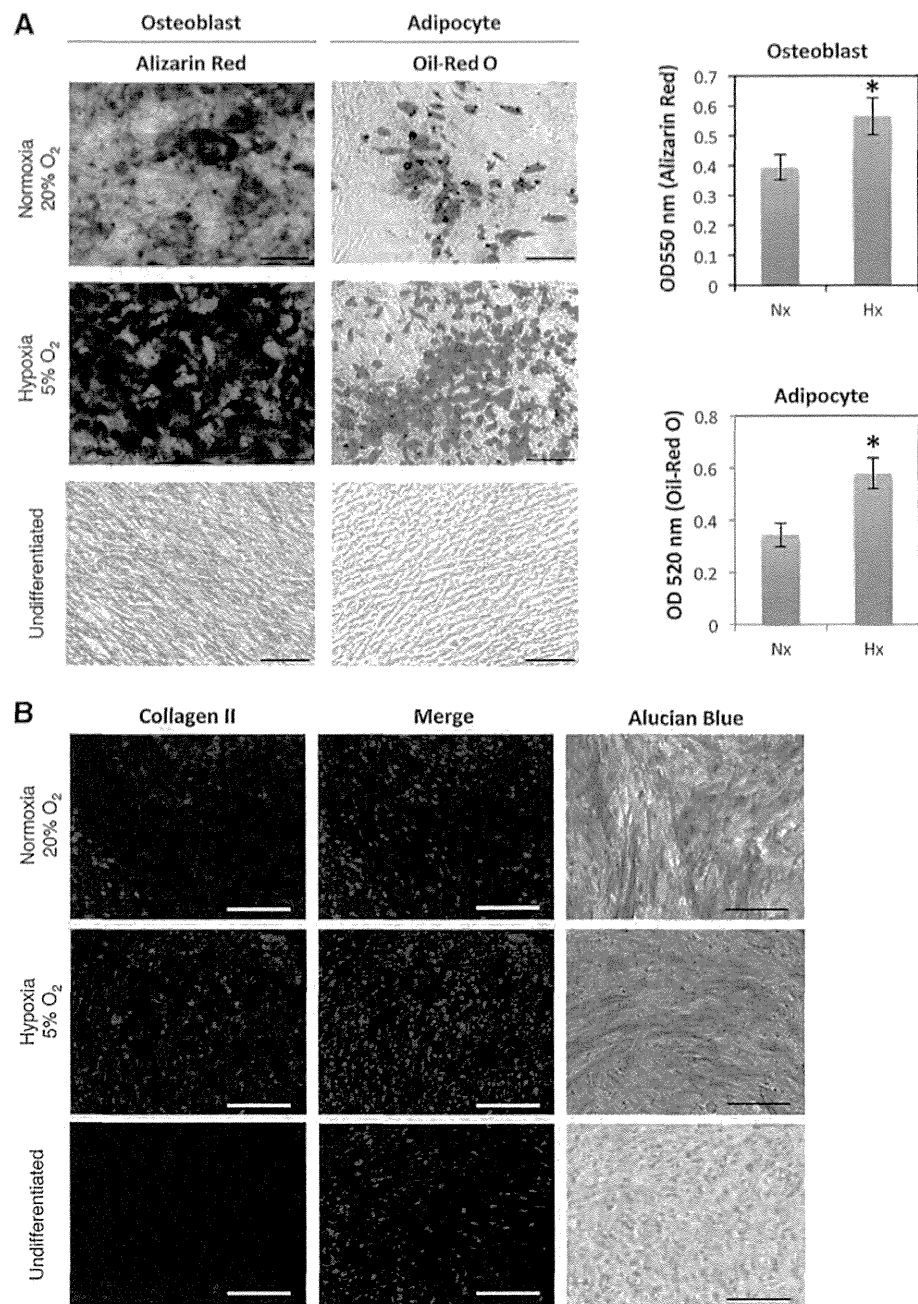
To identify the signaling responsible for the observed effect, we next examined the Akt, NF-κB, and p53 signaling pathways. It has been reported that hypoxic conditions induce the activation of Akt and NF-κB signaling [42,43]. In addition, hypoxic conditions have been shown to inhibit p53 activity [44], and crosstalk between these pathways and Notch signaling has also been demonstrated [41,45–47]. As shown in Fig. 4F, the Hx condition increased Akt phosphorylation, which was not decreased by DAPT treatment. These data demonstrate that 5% oxygen activated Akt signaling but not via Notch signaling. Similarly, the hypoxic condition induced nuclear accumulation of p65, which was

inhibited by DAPT treatment (Fig. 4G). These data suggest that NF-κB signaling is regulated by Notch signaling in hADMPCs. Furthermore, p53 was not activated under the 5% oxygen condition as assessed by detection of phospho-p53 and a p53 reporter assay. However, DAPT treatment significantly increased p53 activity (Fig. 4H, I).

Notch signaling is indispensable for acquisition of the advantageous properties of hADMPCs

We next examined the roles of Notch signaling in the proliferative capacity and stem cell properties of hADMPCs
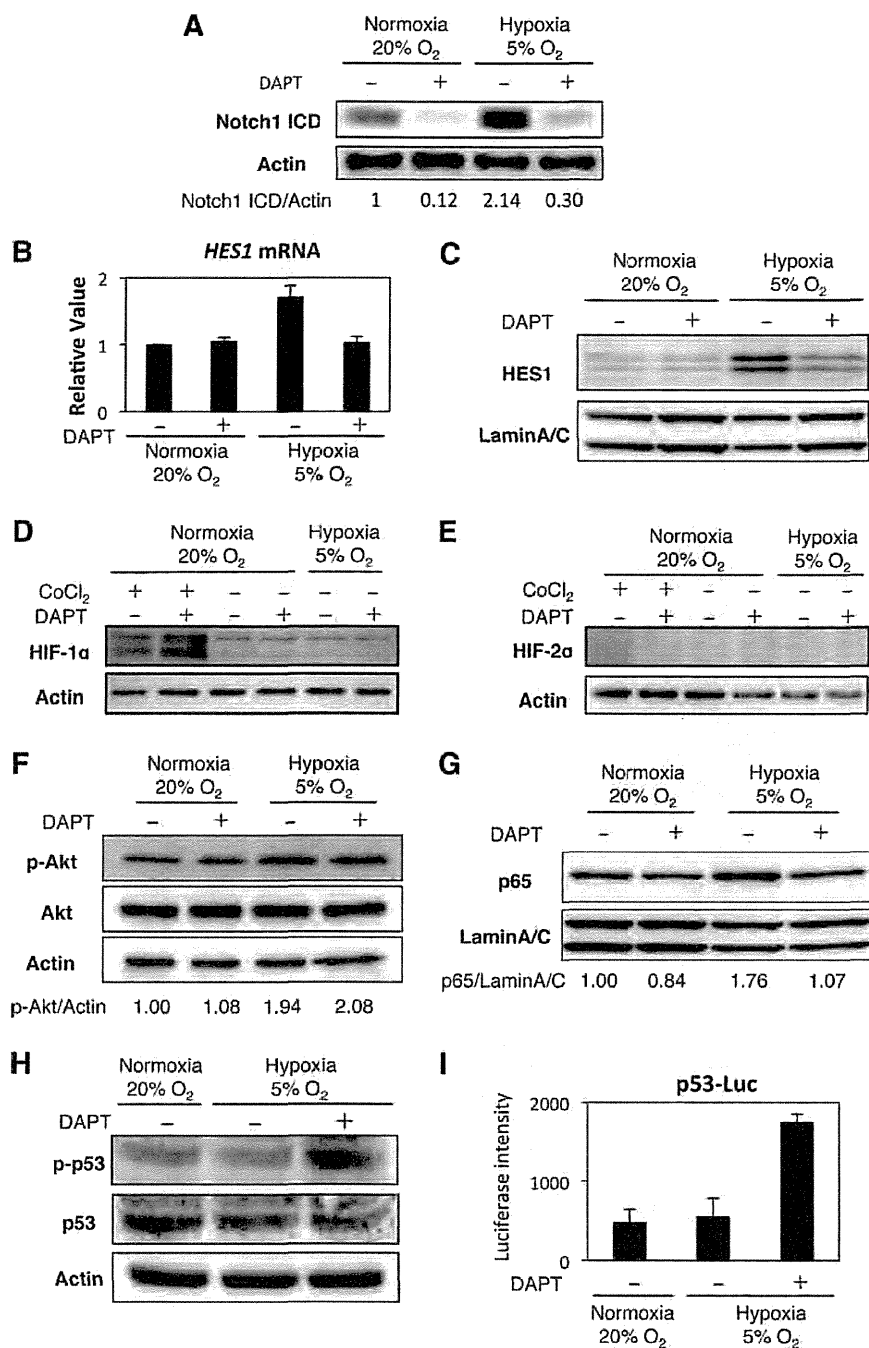
FIG. 4. Hypoxic culture condition activates Notch signaling but not HIF proteins. hADMPCs were expanded under normoxic (20% O₂) and hypoxic (5% O₂) conditions. DAPT (1 μM) was added to inhibit Notch signaling. **(A)** Western blot analysis of intracellular domain of Notch1 (Notch1 ICD) expression. Actin served as the loading control. Numbers below blots indicate relative band intensities as determined by ImageJ software. **(B)** Q-PCR analysis of *HES1*. Each expression value was calculated with the $\Delta\Delta$Ct method using *UBE2D2* as an internal control. **(C)** Western blot analysis of HES1 in nuclear fractions of hADMPCs. Lamin A/C served as the loading control. **(D, E)** Western blot analysis of HIF-1α **(D)** and HIF-2α **(E)**. Cobalt chloride (CoCl₂) was added at a concentration of 100 μM to stabilize HIF proteins (positive control). **(F)** Western blot analysis of phosphorylated Akt (p-Akt) and Akt. Actin served as the loading control. Numbers below blots indicate relative band intensities as determined by ImageJ software. **(G)** Western blot analysis of nuclear localization of p65. Lamin A/C served as the loading control. Numbers below blots indicate relative band intensities as determined by ImageJ software. **(H)** Western blot analysis of phosphorylated p53 (p-p53) and p53. Actin served as the loading control. **(I)** Activity of p53 was measured by the p53-luciferase reporter assay. Relative luciferase activity was determined from three independent experiments and normalized to pGL4.74 activity.

in the Hx culture condition. To inhibit Notch signaling, DAPT was added to the medium at a final concentration of 1 μM. DAPT treatment significantly decreased the PDL when hADMPCs were cultured under either 20% or 5% oxygen (Fig. 5A). Intriguingly, measurement of the DNA content in hADMPCs revealed that inhibition of Notch signaling by 1 μM DAPT significantly attenuated the decrease in apoptotic cells in the Hx condition (Fig. 5B). These data suggest that 5% oxygen increases the proliferation capacity of hADMPCs through Notch signaling by

promoting their survival. To examine whether Notch signaling affects the stem cell properties of hADMPCs, differentiation into adipocyte, osteocyte, and chondrocyte lineages was analyzed at passage 8. Hx-cultured hADMPCs underwent greater differentiation into all lineages as described in Fig. 3, whereas application of a Notch inhibitor significantly decreased the differentiation capacity to all lineages (Fig. 5C–E). In addition, SA-β-Gal staining revealed that inhibition of Notch signaling by DAPT remarkably promoted senescence in both the Nx and Hx

FIG. 5. Notch signaling is indispensable for acquisition of the advantageous properties of hADMPCs. hADMPCs were expanded under normoxic (20% O_2; Nx) and hypoxic (5% O_2; Hx) conditions. DAPT (1 μM) was added to inhibit Notch signaling. (**A**) Growth profiles of hADMPCs under Nx (*red*) and Hx (*blue*) conditions. *Solid lines* represent control cells, and *dotted lines* represent DAPT-treated cells. The number of population doublings was calculated based on the total cell number at each passage. (**B**) Percentages of apoptotic cells with sub-G1 DNA. Results are presented as the mean of three independent experiments ± SD. (**C, D**) hADMPCs at passage 8 were induced for 3 weeks to differentiate into adipocytes (**C**) and osteoblasts (**D**) and stained with Oil Red O and Alizarin Red, respectively. The stained dye was extracted, and OD values were measured and plotted as the means of three independent experiments ± SD. (**E**) hADMPCs at passage 8 were induced for 3 weeks to differentiate into chondrocytes, and an immunofluorescent analysis of collagen II (*red*) was performed. The *blue* signals indicate nuclear staining. (**F**) hADMPCs were stained with SA-β-gal. *$P<0.05$ and **$P<0.01$ indicate significant differences (independent *t*-test) between Nx and Hx. Scale bars; 100 μm. Color images available online at www .liebertpub.com/scd
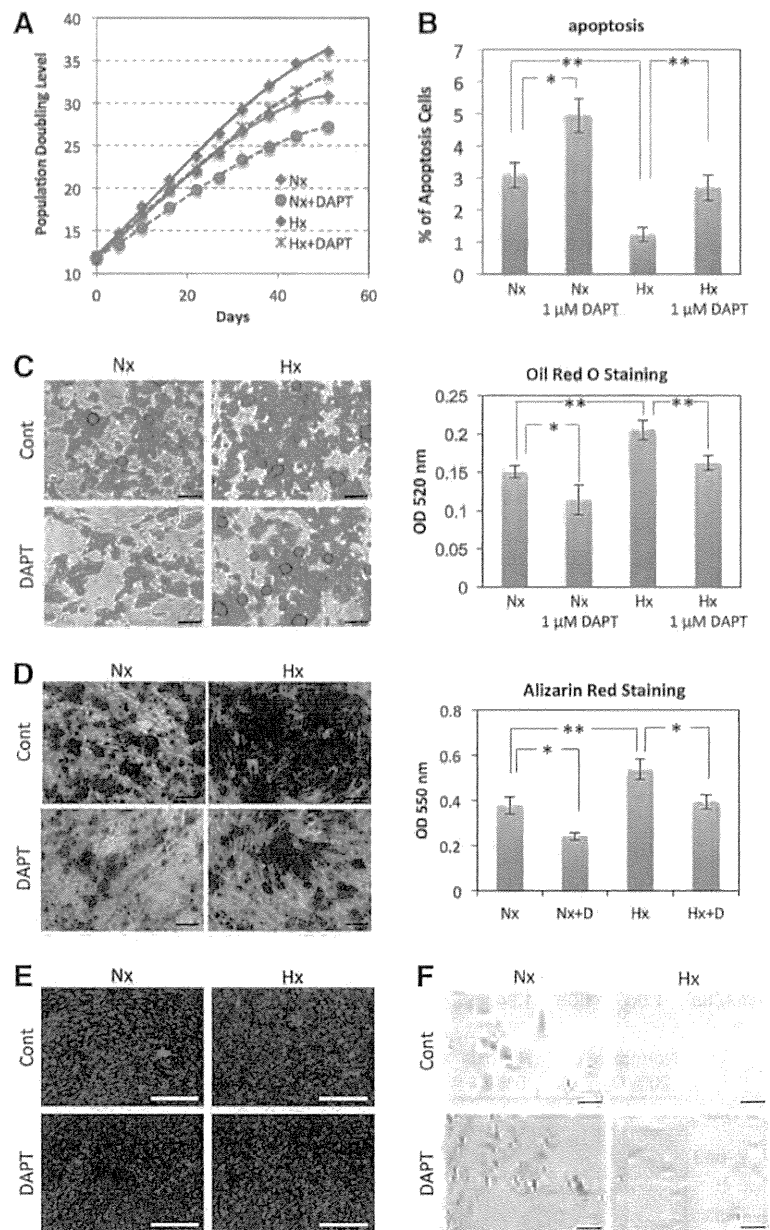
culture conditions, suggesting that the suppression of replicative senescence observed in the Hx condition is mediated by Notch signaling (Fig. 5F).

Glycolysis is enhanced in the 5% oxygen condition through Notch signaling

Recent studies suggest that the metabolic shift from aerobic mitochondrial respiration to glycolysis extends the life span possibly via reduction of intrinsic ROS production [18,19]. Our results demonstrate that the 5% oxygen condition reduced ROS accumulation in hADMPCs (Fig. 1F). In addition, the relationship between Notch signaling and glycolysis has been recently established [48,49]. We, therefore, considered glycolytic flux by measuring the glu-

cose consumption and lactate production of hADMPCs in the Nx or Hx culture conditions. As shown in Fig. 6A, glucose consumption and lactate production were elevated in the Hx culture condition, indicating that a metabolic shift to glycolysis occurred when hADMPCs were cultured in 5% oxygen. In contrast, the Notch inhibitor DAPT markedly reduced glycolytic flux as assessed by glucose consumption and lactate production (Fig. 6A). To identify the genes responsible for the glycolytic change, we performed a Q-PCR analysis. As shown in Fig. 6B, *SLC2A3, TPI, and PGK1*, encoding glycolytic enzymes, were upregulated in the 5% oxygen condition; whereas these genes were suppressed by DAPT treatment. Interestingly, Hes1 transduction by an adenoviral vector markedly induced the mRNA expression of the same genes (Fig. 6E). In addition, SCO2, a positive
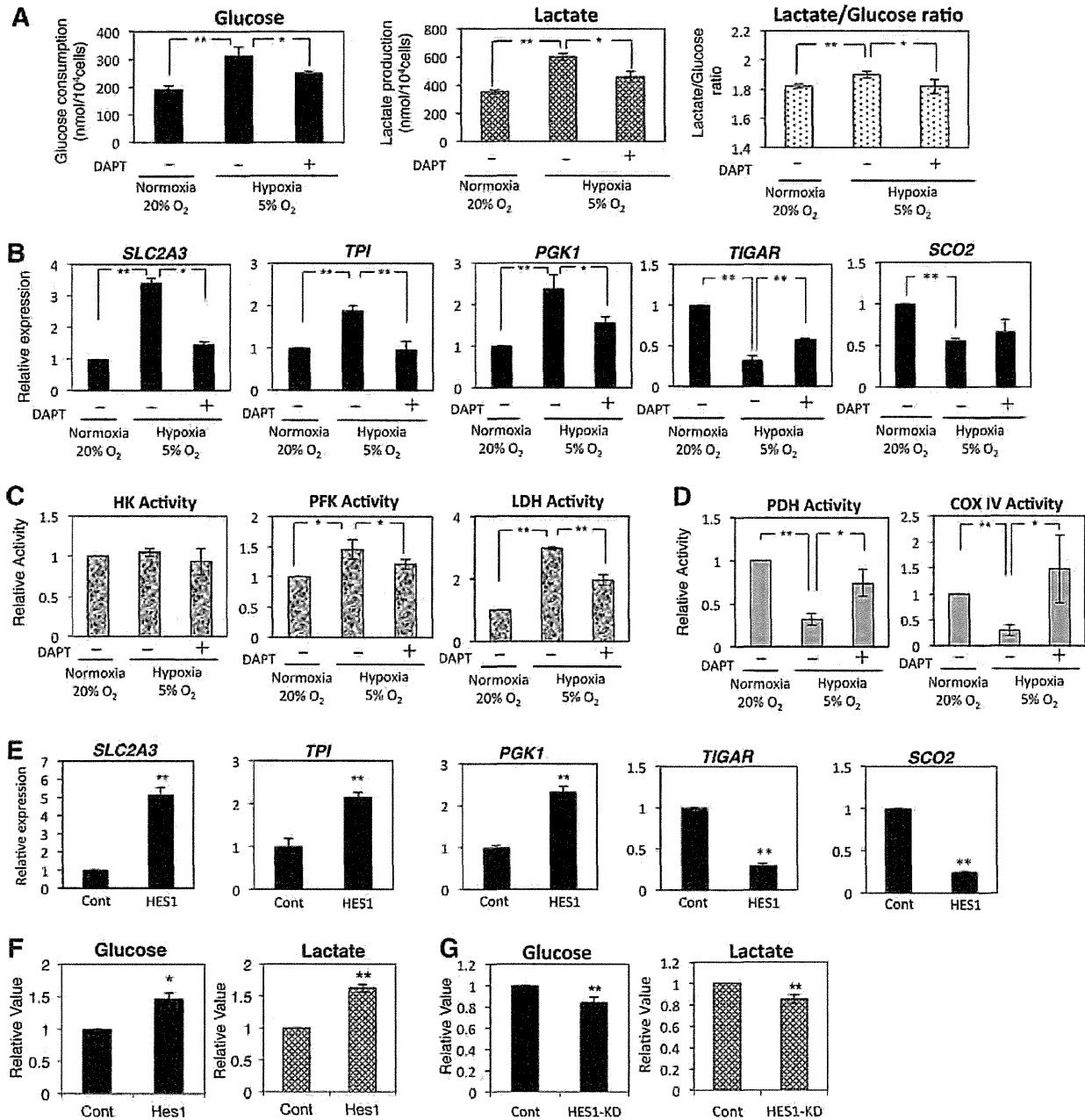
FIG. 6. Glycolysis is enhanced under 5% oxygen through Notch signaling. (A–D) hADMPCs were expanded under normoxic (20% O_2) and hypoxic (5% O_2) conditions. DAPT (1 μM) was added to inhibit Notch signaling. (A) Glucose consumption and lactate production of hADMPCs were measured and plotted as the means of three independent experiments ± SD. (B) Relative mRNA expression of SLC2A3, TPI, PGK1, TIGAR, and SCO2 in hADMPCs. Each expression value was calculated with the ΔΔCt method using UBE2D2 as an internal control. (C, D) Hexokinase (HK), phospho-fructokinase (PFK), lactate dehydrogenase (LDH) (C), pyruvate dehydrogenase (PDH), and Complex IV (Cox IV) (D) activities were measured and the value of relative activity was plotted as the means of three independent experiments ± SD. (E, F) hADMPCs were transduced with either mock (Cont) or HES1 and then cultured for 3 days. (E) Relative mRNA expression of SLC2A3, TPI, PGK1, TIGAR, and SCO2 in hADMPCs. Each expression value was calculated with the ΔΔCt method using UBE2D2 as an internal control. (F) Glucose consumption and lactate production of hADMPCs were measured and plotted as the means of three independent experiments ± SD. (G) hADMPCs were transduced with either scrambled control RNAi (Cont) or RNAi against HES1 (HES1-KD), and then cultured for 3 days. Glucose consumption and lactate production of hADMPCs were measured and plotted as the means of three independent experiments ± SD. $**P < 0.01$. $*0.01 < P < 0.05$.
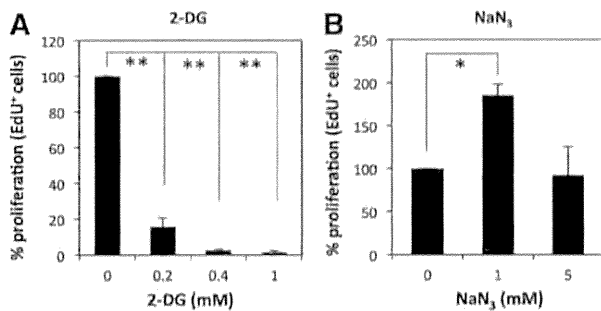
FIG. 7. Glycolysis supports proliferation of hADMPCs. hADMPCs were treated with 0, 0.2, 0.4, and 1 mM 2-deoxy-D-glucose (2-DG) (**A**) or 0, 1, and 5 mM sodium azide (NaN$_3$) (**B**) for 24 h. Cells were then allowed to incorporate EdU for 2 h, and the EdU-positive cells were analyzed by flow cytometry. The percentages for the 0 mM control were plotted as the means of three independent experiments ± SD. *$P < 0.05$; **$P < 0.01$.

modulator of aerobic respiration, and TIGAR, a negative regulator of glycolysis, were transcriptionally downregulated in the 5% oxygen condition; whereas DAPT treatment partially restored the expression level (Fig. 6B). Adenoviral expression of Hes1 dramatically reduced *SCO2* and *TIGAR* expression (Fig. 6E), which suggests that the Notch-Hes1 signaling modulates the metabolic pathway. We also measured the activities of key enzymes in glycolysis. Hexokinase activity was not changed under hypoxic conditions; however, PFK and LDH were activated in 5% oxygen condition, which was attenuated by Notch inhibition (Fig. 6C). In addition, pyruvate dehydrogenase (PDH) and cytochrome c oxidase (Complex IV) activity assays showed that mitochondrial respiration decreased under the hypoxic condition and that DAPT treatment restored it (Fig. 6D). Moreover, glycolytic flux in Hes1-expressing hADMPCs was positively correlated with the expression of these glycolytic genes as assessed by glucose consumption and lactate production (Fig. 6F). In contrast, HES1 knockdown by adenoviral transduction of *HES1* RNAi resulted in a significant reduction of glycolytic flux (Fig. 6G), demonstrating that HES1 is involved in the regulation of glycolysis.

Glycolysis supports the proliferation of hADMPCs

To determine whether aerobic glycolysis is important for the proliferation of hADMPCs, hADMPCs were treated with the glycolytic inhibitor 2-deoxy-D-glucose (2-DG) or the respiration inhibitor sodium azide (NaN$_3$). We found that hADMPCs were sensitive to treatment with 2-DG even at a low concentration of 0.2 mM (Fig. 7A). In contrast, treatment of hADMPCs with NaN$_3$ rather increased their proliferation at the concentration of 1 mM and supported their proliferation even at the concentration of 5 mM (Fig. 7B). These data suggest that the proliferation of hADMPCs is compromised when aerobic glycolysis is blocked.

Discussion

Recent evidence suggests that hypoxic culture conditions confer a growth advantage, prevent premature senescence, and maintain undifferentiated states in ESCs, iPSCs, and

somatic stem cells. However, the molecular mechanism underlying the beneficial effects of culturing these cells at low oxygen conditions remains unclear. Our findings prompted us to hypothesize that Notch signaling in physiological hypoxic conditions (5% O$_2$) contributes to these effects on hADMPCs by modulating glycolytic flux.

We found that 5% O$_2$ significantly increased the proliferation capacity, decreased apoptosis, and inhibited senescence of hADMPCs (Fig. 1). Moreover, 5% O$_2$ improved the differentiation of hADMPCs without affecting the expression of their cell surface markers (Figs. 2 and 3). Welford et al. reported that HIF-1α delays premature senescence of mouse embryonic fibroblasts under hypoxic conditions (2% O$_2$) [50]. Tsai et al. reported that hypoxia (1% O$_2$) inhibits senescence and maintains MSC properties through accumulation of HIF-1α [26]. Hypoxia was recently reported to enhance the undifferentiated status and stem cell properties in various stem and precursor cell populations via the interaction of HIF with the Notch intracellular domain to activate Notch-responsive promoters [38]. In the current study, the effects observed in 5% O$_2$ condition were independent of HIF proteins, because accumulation of HIF-1α and HIF-2α was not observed (Fig. 4). Instead, our findings suggest that 5% O$_2$ activated Notch signaling, which contributed advantageous effects of hypoxic culture on hADMPCs. A pharmacological inhibitor of Notch signaling, DAPT, abrogated the hypoxic-induced Notch activation, increased proliferation capacity and lifespan, maintenance of stem cell properties, and prevention of senescence (Figs. 4 and 5). Moreover, we also found that 5% O$_2$ enhanced glucose consumption and lactate production, and these effects were also attenuated by Notch inhibition (Fig. 6A) and knockdown of HES1 (Fig. 6G). Previously, it has been reported that Notch signaling promotes glycolysis by activating the PI(3)K-Akt pathway [48,49]. However, our results indicate that Akt signaling was not activated by Notch signaling, because DAPT did not attenuate hypoxia-induced Akt phosphorylation (Fig. 4F). Although Akt is unlikely to be regulated by Notch signaling in hADMPCs, it is obvious in our data that Akt signaling was activated by 5% O$_2$. Therefore, we could not rule out the possibility that the promotion of glycolysis in the 5% O$_2$ condition was caused by Akt signaling.

Recent evidence suggests that Notch signaling acts as a metabolic switch [48,51]. Zhou et al. demonstrated that hairy, a basic helix-loop-helix transcriptional repressor regulated by Notch signaling, was upregulated and genes encoding metabolic enzymes, including TCA cycle enzymes and respiratory chain complexes, were downregulated in hypoxia-tolerant flies. Intriguingly, they also found that hairy-binding elements were present in the regulatory region of the downregulated metabolic genes. Their work, thus, provides new evidence that hairy acts as a metabolic switch [51]. Landor et al. demonstrated that both hyper- and hypoactive Notch signaling induced glycolysis, albeit by different mechanisms. They showed that Notch activation increased glycolysis through activation of PI3K-AKT signaling, whereas decreased Notch activity inhibited mitochondrial function in a p53-dependent manner in MCF7 breast cancer cell lines [48]. Consistent with their reports, our findings that Notch signaling promoted activity of some glycolysis enzymes and inhibited mitochondrial activity

(Fig. 6) also suggest that Notch signaling functioned as a metabolic switch. While our data showed that Notch inhibition by DAPT resulted in reduced glycolysis (Fig. 6A–C), induction of mitochondrial function (Fig. 6D) and activation of p53 (Fig. 4H, I) are not consistent with the report of Landor el al. This contradiction might be explained by the expression level of endogenous Notch. Landor et al. showed that in breast cancer MDA-M-231 cells, which showed higher endogenous Notch activity, high glucose uptake, and lactate production than MCF7 breast cancer cell lines, Notch inhibition by DAPT significantly reduced glucose consumption and lactate production [48]. As shown in Fig. 4A, we observed that hADMPCs in 5% O_2 displayed high Notch activity. Moreover, the lactate-to-glucose ratio was 1.8–1.9 in hADMPCs, suggesting that hADMPCs largely rely on glycolysis for energy production (Fig. 6A). In addition, it was reported that hMSCs showed a higher glycolytic rate than primary human fibroblast [52]. It appears that hADMPCs cultured under hypoxic conditions might possess cell properties similar to MDA-M-231 cells or MCF7 cells, in which stable expression of constructs NICD1-GFP produces high Notch activity.

Nuclear translocation of p65 was observed in hypoxic conditions, demonstrating that NF-κB is a direct target of Notch signaling (Fig. 4G). Intriguingly, the hypoxic culture conditions in this study upregulated several genes encoding glycolytic enzymes (*SLC2A3, TPI, and PGK1*); whereas the expression of these genes was suppressed by Notch inhibition. In addition, Hes1 transduction induced mRNA expression of the same genes (Fig. 6). It was previously reported that *SLC2A3* expression was regulated by p65/NF-κB signaling, and that Notch/Hes1 is able to induce the activation of the NF-κB pathway in human T-ALL lines and animal disease models [53]. Espinosa et al. demonstrated that Hes1 directly targeted the deubiquitinase CYLD, resulting in deubiquitination and inactivation of TAK1 and IKK, degradation of IκBa, and activation of NF-κB signaling [53]. In our systems, however, we did not observe repression of *CYLD* mRNA in Hes1-overexpressing hADMPCs (data not shown). While *PGK1* mRNA has been reported to be upregulated by NF-κB, it has not clearly been shown to be controlled by NF-κB despite the presence of an NF-κB site in the promoter [54]. Although modulation of *TPI* expression by NF-κB has not been reported, we found several NF-κB binding sites on the human *TPI* promoter (data not shown). Since NF-κB is likely to be one of the responsible signals for hypoxic-induced glycolysis [53], further analysis will be required to determine the mechanism by which NF-κB signaling is induced by Notch signaling. In addition, it will be important to investigate whether NF-κB is really responsible for the observed glycolysis and whether it regulates the expression of *SLC2A3, TPI*, and *PGK1* in hADMPCs under 5% oxygen.

In addition, SCO2, a positive modulator of aerobic respiration, and TIGAR, a negative regulator of glycolysis, were transcriptionally downregulated in the 5% oxygen condition; whereas DAPT treatment partially restored expression (Fig. 6B). We observed some glycolysis and mitochondrial enzyme activity and found that the activities of COX IV and PFK were consistent with gene expression data (Fig. 6C, D). Adenoviral expression of Hes1 dramatically reduced *SCO2* and *TIGAR* expression (Fig. 6E), which

suggests that Notch-Hes1 signaling modulates the metabolic pathway. Intriguingly, our results also indicate that Hes1 could suppress the expression of *TIGAR* and *SCO2*, a p53 target gene. It has been reported that Notch signaling suppresses p53 in lymphomagenesis [46]. Moreover, Kim et al. reported that NICD1 inhibits p53 phosphorylation and represses p53 transactivation by interacting with p53 [47]. In addition, DAPT treatment resulted in the enhancement of p53 activity in the hypoxic conditions (Fig. 4H, I). Therefore, it is possible that p53 activation was regulated by Notch signaling in hADMPCs, although we did not observe a decrease in p53 activity in hypoxic conditions in this study (Fig. 4). Further analysis will be required to determine whether p53 activity is suppressed in hypoxic conditions over a longer period of culture.

Cells undergoing active proliferation utilize large amounts of glucose through glycolysis, producing pyruvate for use in substrates (amino acids and lipids) and the pentose shunt for use in nucleic acid substrates, and also producing NADPH as a reducing agent to counter oxidative stress [18,55]. In the current study, 5% O_2 actually increased proliferation and decreased the accumulation of ROS, which may be involved in the reduction of senescence (Fig. 1). Since accumulation of endogenous ROS might be a major reason for replicative senescence [20], enhancing glycolysis in cultured cells may improve the quality of the cells by suppressing premature senescence. Kondoh et al. demonstrated that enhanced glycolysis is involved in cellular immortalization through reduction of intrinsic ROS production [14,18,19]. Therefore, it is possible that the extension of lifespan observed in our experimental conditions was caused by the reduction of intracellular ROS levels through enhanced glycolysis by Notch signaling. Our data indicate that aerobic glycolysis is utilized for proliferation of hADMPCs, because the glycolytic inhibitor 2-DG attenuates the proliferation rate of hADMPCs (Fig. 7A). Intriguingly, the aerobic respiration block by NaN_3 did not decrease the proliferation; rather, it increased proliferation at a low concentration (Fig. 7B), which may support our data indicating that the metabolic switch from mitochondrial respiration to glycolysis provides a growth advantage to hADMPCs. However, the question of whether the enhanced glycolysis really contributes to the prolonged lifespan in hADMPCs remains to be determined in this study.

In the current study, the molecular mechanism for how Notch signaling is activated in 5% O_2 conditions was explored. It has been reported that Notch1 activity is influenced by oxygen concentration [40,41,56]. In melanoma cells, hypoxia (2% O_2) resulted in increased expression of Notch1 by HIF-1α and also by Akt through NF-κB activity [41]. Similarly, in hypoxic breast cancer cells, Notch ligand JAG2 was shown to be transcriptionally activated by hypoxia (1% O_2) in an HIF-1α-dependent manner, resulting in an elevation of Notch signaling [40]. In contrast, in hESCs continuously cultured in 5% O_2, alteration of the Notch pathway seems to be independent of HIF-1α [56]. In our system, Notch1 activation was not likely dependent on HIF-1α and HIF-2α, because these proteins did not accumulate in the Hx condition. In contrast, our results indicate that the 5% O_2 condition activated Akt and NF-κB signaling (Fig. 4), which suggests that these molecules may activate Notch signaling in hADMPCs. NF-κB was previously shown to

increase Notch1 activity indirectly by increasing the expression of Notch ligand Jagged1 in HeLa, lymphoma, and myeloma cells [57]. In addition, Akt regulated Notch1 by increasing Notch1 transcription through the activity of NF-κB in melanoma cells [41]. Further analysis is required to clarify the mechanism underlying this phenomenon.

In conclusion, the 5% oxygen condition conferred a growth advantage through a metabolic shift to glycolysis, improved the proliferation efficiency, prevented the cellular senescence, and maintained the undifferentiated status of hADMPCs. These observations, thus, provide new regulatory mechanisms for the maintenance of stemness observed in 5% oxygen conditions. In addition, our study sheds new light on the regulation of replicative senescence, which might have an impact for quality control of hADMPC preparations used for therapeutic applications.

Acknowledgments

Author Disclosure Statement

The authors declare no conflict of interest. No competing financial interests exist.

References

1. Okura H, H Komoda, A Saga, A Kakuta-Yamamoto, Y Hamada, Y Fumimoto, CM Lee, A Ichinose, Y Sawa and A Matsuyama. (2010). Properties of hepatocyte-like cell clusters from human adipose tissue-derived mesenchymal stem cells. Tissue Eng Part C Methods 16:761–770.

2. Okura H, A Matsuyama, CM Lee, A Saga, A Kakuta-Yamamoto, A Nagao, N Sougawa, N Sekiya, K Takekita, et al. (2010). Cardiomyoblast-like cells differentiated from human adipose tissue-derived mesenchymal stem cells improve left ventricular dysfunction and survival in a rat myocardial infarction model. Tissue Eng Part C Methods 16:417–425.

3. Okura H, H Komoda, Y Fumimoto, CM Lee, T Nishida, Y Sawa and A Matsuyama. (2009). Transdifferentiation of human adipose tissue-derived stromal cells into insulin-producing clusters. J Artif Organs 12:123–130.

4. Safford KM, SD Safford, JM Gimble, AK Shetty and HE Rice. (2004). Characterization of neuronal/glial differentiation of murine adipose-derived adult stromal cells. Exp Neurol 187:319–328.

5. Leu S, YC Lin, CM Yuen, CH Yen, YH Kao, CK Sun and HK Yip. (2010). Adipose-derived mesenchymal stem cells markedly attenuate brain infarct size and improve neurological function in rats. J Transl Med 8:63.

6. Ikegame Y, K Yamashita, S Hayashi, H Mizuno, M Tawada, F You, K Yamada, Y Tanaka, Y Egashira, et al. (2011). Comparison of mesenchymal stem cells from adipose tissue and bone marrow for ischemic stroke therapy. Cytotherapy 13:675–685.

7. Tan B, Z Luan, X Wei, Y He, G Wei, BH Johnstone, M Farlow and Y Du. (2011). AMP-activated kinase mediates adipose stem cell-stimulated neuritogenesis of PC12 cells. Neuroscience 181:40–47.

8. Reid AJ, M Sun, M Wiberg, S Downes, G Terenghi and PJ Kingham. (2011). Nerve repair with adipose-derived stem cells protects dorsal root ganglia neurons from apoptosis. Neuroscience 199:515–522.

9. Rehman J, D Traktuev, J Li, S Merfeld-Clauss, CJ Temm-Grove, JE Bovenkerk, CL Pell, BH Johnstone, RV Considine and KL March. (2004). Secretion of angiogenic and antiapoptotic factors by human adipose stromal cells. Circulation 109:1292–1298.

10. Lee EY, Y Xia, WS Kim, MH Kim, TH Kim, KJ Kim, BS Park and JH Sung. (2009). Hypoxia-enhanced wound-healing function of adipose-derived stem cells: increase in stem cell proliferation and up-regulation of VEGF and bFGF. Wound Repair Regen 17:540–547.

11. Moriyama M, H Moriyama, A Ueda, Y Nishibata, H Okura, A Ichinose, A Matsuyama and T Hayakawa. (2012). Human adipose tissue-derived multilineage progenitor cells exposed to oxidative stress induce neurite outgrowth in PC12 cells through p38 MAPK signaling. BMC Cell Biol 13:21.

12. Wu H, Z Ye and RI Mahato. (2011). Genetically modified mesenchymal stem cells for improved islet transplantation. Mol Pharm 8:1458–1470.

13. Wagner W, P Horn, M Castoldi, A Diehlmann, S Bork, R Saffrich, V Benes, J Blake, S Pfister, V Eckstein and AD Ho. (2008). Replicative senescence of mesenchymal stem cells: a continuous and organized process. PLoS One 3:e2213.

14. Kondoh H, ME Lleonart, Y Nakashima, M Yokode, M Tanaka, D Bernard, J Gil and D Beach. (2007). A high glycolytic flux supports the proliferative potential of murine embryonic stem cells. Antioxid Redox Signal 9:293–299.

15. Prigione A, B Fauler, R Lurz, H Lehrach and J Adjaye. (2010). The senescence-related mitochondrial/oxidative stress pathway is repressed in human induced pluripotent stem cells. Stem Cells 28:721–733.

16. Varum S, AS Rodrigues, MB Moura, O Momcilovic, C At Easley, J Ramalho-Santos, B Van Houten and G Schatten. (2011). Energy metabolism in human pluripotent stem cells and their differentiated counterparts. PLoS One 6:e20914.

17. Warburg O, F Wind and E Negelein. (1927). The Metabolism of tumors in the body. J Gen Physiol 8:519–530.

18. Kondoh H. (2008). Cellular life span and the Warburg effect. Exp Cell Res 314:1923–1928.

19. Kondoh H, ME Lleonart, J Gil, J Wang, P Degan, G Peters, D Martinez, A Carnero and D Beach. (2005). Glycolytic enzymes can modulate cellular life span. Cancer Res 65:177–185.

20. Beckman KB and BN Ames. (1998). The free radical theory of aging matures. Physiol Rev 78:547–581.

21. Ezashi T, P Das and RM Roberts. (2005). Low O2 tensions and the prevention of differentiation of hES cells. Proc Natl Acad Sci U S A 102:4783–4788.

22. Forristal CE, KL Wright, NA Hanley, RO Oreffo and FD Houghton. (2010). Hypoxia inducible factors regulate pluripotency and proliferation in human embryonic stem cells cultured at reduced oxygen tensions. Reproduction 139:85–97.

23. Yoshida Y, K Takahashi, K Okita, T Ichisaka and S Yamanaka. (2009). Hypoxia enhances the generation of induced pluripotent stem cells. Cell Stem Cell 5:237–241.

24. Takubo K, N Goda, W Yamada, H Iriuchishima, E Ikeda, Y Kubota, H Shima, RS Johnson, A Hirao, M Suematsu and T Suda. (2010). Regulation of the HIF-1alpha level is essential for hematopoietic stem cells. Cell Stem Cell 7:391–402.

25. Santilli G, G Lamorte, L Carlessi, D Ferrari, L Rota Nodari, E Binda, D Delia, AL Vescovi and L De Filippis. (2010). Mild hypoxia enhances proliferation and multipotency of human neural stem cells. PLoS One 5:e8575.

26. Tsai CC, YJ Chen, TL Yew, LL Chen, JY Wang, CH Chiu and SC Hung. (2011). Hypoxia inhibits senescence and maintains mesenchymal stem cell properties through down-regulation of E2A-p21 by HIF-TWIST. Blood 117:459–469.

27. Takubo K, G Nagamatsu, CI Kobayashi, A Nakamura-Ishizu, H Kobayashi, E Ikeda, N Goda, Y Rahimi, RS Johnson, et al. (2013). Regulation of glycolysis by pdk functions as a metabolic checkpoint for cell cycle quiescence in hematopoietic stem cells. Cell Stem Cell 12:49–61.

28. Grayson WL, F Zhao, R Izadpanah, B Bunnell and T Ma. (2006). Effects of hypoxia on human mesenchymal stem cell expansion and plasticity in 3D constructs. J Cell Physiol 207:331–339.

29. Wang DW, B Fermor, JM Gimble, HA Awad and F Guilak. (2005). Influence of oxygen on the proliferation and metabolism of adipose derived adult stem cells. J Cell Physiol 204:184–191.

30. Moriyama M, M Osawa, SS Mak, T Ohtsuka, N Yamamoto, H Han, V Delmas, R Kageyama, F Beermann, L Larue and S Nishikawa. (2006). Notch signaling via Hes1 transcription factor maintains survival of melanoblasts and melanocyte stem cells. J Cell Biol 173:333–339.

31. Chiba S. (2006). Notch signaling in stem cell systems. Stem Cells 24:2437–2447.

32. Okura H, A Saga, Y Fumimoto, M Soeda, M Moriyama, H Moriyama, K Nagai, CM Lee, S Yamashita, et al. (2011). Transplantation of human adipose tissue-derived multi-lineage progenitor cells reduces serum cholesterol in hyperlipidemic Watanabe rabbits. Tissue Eng Part C Methods 17:145–154.

33. Saga A, H Okura, M Soeda, J Tani, Y Fumimoto, H Komoda, M Moriyama, H Moriyama, S Yamashita, et al. (2011). HMG-CoA reductase inhibitor augments the serum total cholesterol-lowering effect of human adipose tissue-derived multilineage progenitor cells in hyperlipidemic homozygous Watanabe rabbits. Biochem Biophys Res Commun 412:50–54.

34. Moriyama H, M Moriyama, K Sawaragi, H Okura, A Ichinose, A Matsuyama and T Hayakawa. (2013). Tightly regulated and homogeneous transgene expression in human adipose-derived mesenchymal stem cells by lentivirus with tet-off system. PLoS One 8:e66274.

35. Sekiya I, BL Larson, JR Smith, R Pochampally, JG Cui and DJ Prockop. (2002). Expansion of human adult stem cells from bone marrow stroma: conditions that maximize the yields of early progenitors and evaluate their quality. Stem Cells 20:530–541.

36. Wagner W, F Wein, A Seckinger, M Frankhauser, U Wirkner, U Krause, J Blake, C Schwager, V Eckstein, W Ansorge and AD Ho. (2005). Comparative characteristics of mesenchymal stem cells from human bone marrow, adipose tissue, and umbilical cord blood. Exp Hematol 33:1402–1416.

37. Hass R, C Kasper, S Bohm and R Jacobs. (2011). Different populations and sources of human mesenchymal stem cells (MSC): A comparison of adult and neonatal tissue-derived MSC. Cell Commun Signal 9:12.

38. Gustafsson MV, X Zheng, T Pereira, K Gradin, S Jin, J Lundkvist, JL Ruas, L Poellinger, U Lendahl and M Bondesson. (2005). Hypoxia requires notch signaling to maintain the undifferentiated cell state. Dev Cell 9:617–628.

39. Zheng X, S Linke, JM Dias, X Zheng, K Gradin, TP Wallis, BR Hamilton, M Gustafsson, JL Ruas, et al. (2008). Interaction with factor inhibiting HIF-1 defines an additional mode of cross-coupling between the Notch and hypoxia signaling pathways. Proc Natl Acad Sci U S A 105:3368–3373.

40. Pietras A, K von Stedingk, D Lindgren, S Pahlman and H Axelson. (2011). JAG2 induction in hypoxic tumor cells alters Notch signaling and enhances endothelial cell tube formation. Mol Cancer Res 9:626–636.

41. Bedogni B, JA Warneke, BJ Nickoloff, AJ Giaccia and MB Powell. (2008). Notch1 is an effector of Akt and hypoxia in melanoma development. J Clin Invest 118:3660–3670.

42. Beitner-Johnson D, RT Rust, TC Hsieh and DE Millhorn. (2001). Hypoxia activates Akt and induces phosphorylation of GSK-3 in PC12 cells. Cell Signal 13:23–27.

43. Culver C, A Sundqvist, S Mudie, A Melvin, D Xirodimas and S Rocha. (2010). Mechanism of hypoxia-induced NF-kappaB. Mol Cell Biol 30:4901–4921.

44. Rohwer N, C Dame, A Haugstetter, B Wiedenmann, K Detjen, CA Schmitt and T Cramer. (2010). Hypoxia-inducible factor 1alpha determines gastric cancer chemosensitivity via modulation of p53 and NF-kappaB. PLoS One 5:e12038.

45. Espinosa L, S Cathelin, T D'Altri, T Trimarchi, A Statnikov, J Guiu, V Rodilla, J Ingles-Esteve, J Nomdedeu, et al. (2010). The Notch/Hes1 pathway sustains NF-kappaB activation through CYLD repression in T cell leukemia. Cancer Cell 18:268–281.

46. Beverly LJ, DW Felsher and AJ Capobianco. (2005). Suppression of p53 by Notch in lymphomagenesis: implications for initiation and regression. Cancer Res 65:7159–7168.

47. Kim SB, GW Chae, J Lee, J Park, H Tak, JH Chung, TG Park, JK Ahn and CO Joe. (2007). Activated Notch1 interacts with p53 to inhibit its phosphorylation and trans-activation. Cell Death Differ 14:982–991.

48. Landor SK, AP Mutvei, V Mamaeva, S Jin, M Busk, R Borra, TJ Gronroos, P Kronqvist, U Lendahl and CM Sahlgren. (2011). Hypo- and hyperactivated Notch signaling induce a glycolytic switch through distinct mechanisms. Proc Natl Acad Sci U S A 108:18814–18819.

49. Ciofani M and JC Zuniga-Pflucker. (2005). Notch promotes survival of pre-T cells at the beta-selection checkpoint by regulating cellular metabolism. Nat Immunol 6:881–888.

50. Welford SM, B Bedogni, K Gradin, L Poellinger, M Broome Powell and AJ Giaccia. (2006). HIF1alpha delays premature senescence through the activation of MIF. Genes Dev 20:3366–3371.

51. Zhou D, J Xue, JC Lai, NJ Schork, KP White and GG Haddad. (2008). Mechanisms underlying hypoxia tolerance in Drosophila melanogaster: hairy as a metabolic switch. PLoS Genet 4:e1000221.

52. Funes JM, M Quintero, S Henderson, D Martinez, U Qureshi, C Westwood, MO Clements, D Bourboulia, RB Pedley,

S Moncada and C Boshoff. (2007). Transformation of human mesenchymal stem cells increases their dependency on oxidative phosphorylation for energy production. Proc Natl Acad Sci U S A 104:6223–6228.

53. Kawauchi K, K Araki, K Tobiume and N Tanaka. (2008). p53 regulates glucose metabolism through an IKK-NF-kappaB pathway and inhibits cell transformation. Nat Cell Biol 10:611–618.

54. Carter KL, E Cahir-McFarland and E Kieff. (2002). Epstein-barr virus-induced changes in B-lymphocyte gene expression. J Virol 76:10427–10436.

55. Ak P and AJ Levine. (2010). p53 and NF-kappaB: different strategies for responding to stress lead to a functional antagonism. FASEB J 24:3643–3652.

56. Prasad SM, M Czepiel, C Cetinkaya, K Smigielska, SC Weli, H Lysdahl, A Gabrielsen, K Petersen, N Ehlers, et al. (2009). Continuous hypoxic culturing maintains activation of Notch and allows long-term propagation of human embryonic stem cells without spontaneous differentiation. Cell Prolif 42:63–74.

57. Bash J, WX Zong, S Banga, A Rivera, DW Ballard, Y Ron and C Gelinas. (1999). Rel/NF-kappaB can trigger the Notch signaling pathway by inducing the expression of Jagged1, a ligand for Notch receptors. EMBO J 18:2803–2811.

Address correspondence to:
Dr. Hiroyuki Moriyama
Pharmaceutical Research and Technology Institute
Kinki University
3-4-1 Kowakae
Higashi-Osaka
Osaka 577-8502
Japan

E-mail: moriyama@phar.kindai.ac.jp

BNIP3 Plays Crucial Roles in the Differentiation and Maintenance of Epidermal Keratinocytes

Mariko Moriyama[1,2,4], Hiroyuki Moriyama[1,4], Junki Uda[1], Akifumi Matsuyama[2], Masatake Osawa[3] and Takao Hayakawa[1]

Transcriptome analysis of the epidermis of $Hes1^{-/-}$ mouse revealed the direct relationship between Hes1 (hairy and enhancer of split-1) and BNIP3 (BCL2 and adenovirus E1B 19-kDa-interacting protein 3), a potent inducer of autophagy. Keratinocyte differentiation is going along with activation of lysosomal enzymes and organelle clearance, expecting the contribution of autophagy in this process. We found that BNIP3 was expressed in the suprabasal layer of the epidermis, where autophagosome formation is normally observed. Forced expression of BNIP3 in human primary epidermal keratinocytes (HPEKs) resulted in autophagy induction and keratinocyte differentiation, whereas knockdown of BNIP3 had the opposite effect. Intriguingly, addition of an autophagy inhibitor significantly suppressed the BNIP3-stimulated differentiation of keratinocytes, suggesting that BNIP3 plays a crucial role in keratinocyte differentiation by inducing autophagy. Furthermore, the number of dead cells increased in the human epidermal equivalent of BNIP3 knockdown keratinocytes, which suggests that BNIP3 is important for maintenance of skin epidermis. Interestingly, although UVB irradiation stimulated BNIP3 expression and cleavage of caspase3, suppression of UVB-induced BNIP3 expression led to further increase in cleaved caspase3 levels. This suggests that BNIP3 has a protective effect against UVB-induced apoptosis in keratinocytes. Overall, our data provide valuable insights into the role of BNIP3 in the differentiation and maintenance of epidermal keratinocytes.

INTRODUCTION

The skin epidermis is a stratified epithelium. Stratification is a key process of epidermal development. During epidermal development, the single layer of basal cells undergoes asymmetric cell division to stratify, and produce committed suprabasal cells on the basal layer. These suprabasal cells are still immature and sustain several rounds of cell divisions to form fully stratified epithelia. Recent studies have identified numerous molecules involved in epidermal development, although how these molecules coordinate to induce proper stratification of the epidermis remains to be elucidated. Previously, by integrating both loss- and gain-of-function

[1]Pharmaceutical Research and Technology Institute, Kinki University, Higashi-Osaka, Osaka, Japan; [2]Platform for Realization of Regenerative Medicine, Foundation for Biomedical Research and Innovation, Kobe, Hyogo, Japan and [3]Division of Regeneration Technology, Gifu University School of Medicine, Gifu, Gifu, Japan

[4]These authors contributed equally to this work.

Correspondence: Mariko Moriyama, Pharmaceutical Research and Technology Institute, Kinki University, Higashi-Osaka, Osaka 577-8502, Japan. E-mail: mariko@phar.kindai.ac.jp

Abbreviations: 3-MA, 3-methyladenine; BNIP3, BCL2 and adenovirus E1B 19-kDa-interacting protein 3; ChIP, chromatin immunoprecipitation; Hes1, hairy and enhancer of split-1; HPEK, human primary epidermal keratinocyte; Q-PCR, quantitative PCR

studies of Notch receptors and their downstream target Hes1 (hairy and enhancer of split-1), we demonstrated the multiple roles of Notch signaling in the regulation of suprabasal cells (Moriyama et al., 2008). Notch signaling induces differentiation of suprabasal cells in a Hes1-independent manner, whereas Hes1 is required for maintenance of the immature status of suprabasal cells by preventing premature differentiation. In light of the critical role of Hes1 in the maintenance of spinous cells, exploration of the molecular targets of Hes1 in spinous layer cells may lead to the discovery of the molecules required for differentiation of spinous layer cells to granular layer cells. Because Hes1 is thought to be a transcriptional repressor (Ohtsuka et al., 1999), loss of Hes1 is expected to cause aberrant upregulation of genes that are normally repressed in spinous layer cells. To identify these genes, we previously conducted comparative global transcript analysis using microarrays and found several candidates that may play a crucial role in regulating epidermal development (Moriyama et al., 2008). One of the genes that was highly expressed was BNIP3 (BCL2 and adenovirus E1B 19-kDa-interacting protein 3), an atypical pro-apoptotic BH3-only protein that induces cell death and autophagy (Zhang and Ney, 2009).

The molecular mechanism through which BNIP3 induces cell death is not well understood; however, it has been reported that BNIP3 protein is induced by hypoxia in some tumor cells and that the kinetics of this induction correlate with cell death (Sowter et al., 2001). In contrast,

BNIP3-induced autophagy has been shown to protect HL-1 myocytes from cell death in an ischemia–reperfusion model (Hamacher-Brady *et al.*, 2007). Induction of autophagy by BNIP3 has a protective effect in some conditions, whereas in others it is associated with autophagic cell death. Recent evidence also suggests that BNIP3, through autophagy, is also required for the differentiation of chondrocytes under hypoxic conditions (Zhao *et al.*, 2012).

Autophagy was initially described based on its ultra-structural features of the double-membraned structures that surrounded the cytoplasm and organelles in cells, known as autophagosomes (Mizushima *et al.*, 2010). To date, only microtubule-associated protein light chain 3 (LC3), a mammalian homolog of yeast Atg8, is known to be expressed in autophagosomes and, therefore, it serves as a widely used marker for autophagosomes (Kabeya *et al.*, 2000; Mizushima *et al.*, 2004). Autophagy is an evolutionarily conserved catabolic program that is activated in response to starvation or changing nutrient conditions. Recently, autophagy was shown to be involved in differentiation of multiple cell types, including erythrocytes, lymphocytes, adipocyte, neuron, and chondrocyte (Srinivas *et al.*, 2009; Mizushima and Levine, 2010).

Epidermal cornification, the process of terminal keratinocyte differentiation, requires programmed cell death in a similar but different pathway from apoptosis (Lippens *et al.*, 2005). Cornification is also accompanied by activation of lysosomal enzymes and organelle clearance. Moreover, some researchers have reported that autophagy may play a role in epidermal differentiation (Haruna *et al.*, 2008; Aymard *et al.*, 2011; Chatterjea *et al.*, 2011). Therefore, it is likely that BNIP3 is involved in cornification through cell death or autophagy.

In this study, transcriptome analysis of *Hes1*$^{-/-}$ mouse epidermis revealed that Hes1 could directly suppress BNIP3 expression in epidermal keratinocytes. We also found that BNIP3 was expressed in the suprabasal layer of the human skin epidermis, where autophagosome formation was observed. BNIP3 was also sufficient to promote cornification through induction of autophagy. Finally, we found that BNIP3 had a protective effect against UVB-induced apoptosis in keratinocytes *in vitro*. Our data thus indicate that BNIP3, an inducer of autophagy, is involved in the terminal differentiation and maintenance of epidermal keratinocytes.

RESULTS

Hes1 directly represses BNIP3 expression in epidermal cells and keratinocytes

We previously performed a microarray analysis with epidermal RNAs isolated from wild-type and *Hes1*$^{-/-}$ mice (Moriyama *et al.*, 2008) and found that BNIP3 was preferentially overexpressed in *Hes1*$^{-/-}$ epidermis. The upregulation of *Bnip3* in the *Hes1*$^{-/-}$ epidermis was confirmed by quantitative PCR (Q-PCR) and immunofluorescent staining (Figure 1a and b). As Hes1 is thought to be a transcriptional repressor (Ishibashi *et al.*, 1994), it might play a repressive role in the regulation of BNIP3 expression. In accordance with this hypothesis, BNIP3 expression in *Hes1*$^{-/-}$ epidermis at embryonic day 15.5 was observed in

the suprabasal layers (Figure 1b), where Hes1 has been reported to be expressed in wild-type epidermis at the same age (Blanpain *et al.*, 2006; Moriyama *et al.*, 2008). To confirm whether Hes1 suppresses BNIP3 expression, an adenoviral vector expressing Hes1 was used to infect human primary epidermal keratinocytes (HPEKs) and, subsequently, the expression level of BNIP3 was quantified by Q-PCR and western blot analysis. The BNIP3 protein was detected as multiple bands between 22 and 30 kD as previously reported (Vengellur and LaPres, 2004; Walls *et al.*, 2009; Mellor *et al.*, 2010; Sassone *et al.*, 2010). We found that Hes1 induced a substantial reduction of BNIP3 expression in HPEKs at the mRNA and protein levels (Figure 1c and d), demonstrating that Hes1 is involved in the repression of BNIP3. To determine whether Hes1 directly regulates *BNIP3* expression, we performed chromatin immunoprecipitation (ChIP) assays. We identified at least 5 Hes1 consensus binding sites 1 kb upstream of the transcription initiation site of the human *BNIP3* gene, and subsequent Q-PCR analysis revealed that a DNA fragment located at -247 to -87 was slightly amplified from crosslinked chromatin isolated by Hes1 immunoprecipitation (Figure 1e). We also found an additional site between -212 and $+22$ that was strongly amplified. These data clearly show that Hes1 specifically binds to the promoter region of *BNIP3* and directly suppresses its expression.

BNIP3 is expressed in the granular layer of the epidermis, where autophagosome formation is observed

To determine the BNIP3 expression profile in the epidermis, we performed immunofluorescent staining in human skin epidermal equivalent. BNIP3 was expressed in the granular layer of epidermal equivalent 18 days (Figure 2a and b) or 24 days (Figure 2c and d) after exposure at the air–liquid interface. BNIP3 expression in the granular layer was also observed in the normal human skin epidermis (Figure 2g and h). Recent reports show that BNIP3 is expressed in mitochondria and that it induces autophagy (Quinsay *et al.*, 2010). In addition, some researchers have reported that autophagy may play a role in epidermal differentiation (Haruna *et al.*, 2008; Aymard *et al.*, 2011; Chatterjea *et al.*, 2011). We therefore investigated whether autophagy occurred in the epidermis, especially in the granular layers. To quantitate the level of autophagy, cytosol to membrane translocation of the autophagy marker EGFP-LC3 (Kabeya *et al.*, 2000) was monitored in a human skin equivalent model (Mizushima *et al.*, 2004). When autophagy is active, autophagosomes containing EGFP-LC3 are visible as fluorescent puncta (Kabeya *et al.*, 2000). As expected, EGFP-LC3 puncta were observed in the granular layers of the epidermal equivalent (Figure 2e). Moreover, endogenous LC3 dots were observed in the granular layers of normal human skin epidermis (Figure 2f). These data suggested that BNIP3 might be involved in the induction of autophagy in the granular layer of the epidermis.

BNIP3 is required for terminal differentiation of keratinocyte by induction of autophagy *in vitro*

To investigate the involvement of BNIP3 in the induction of autophagy, we transduced HPEKs stably expressing EGFP-LC3
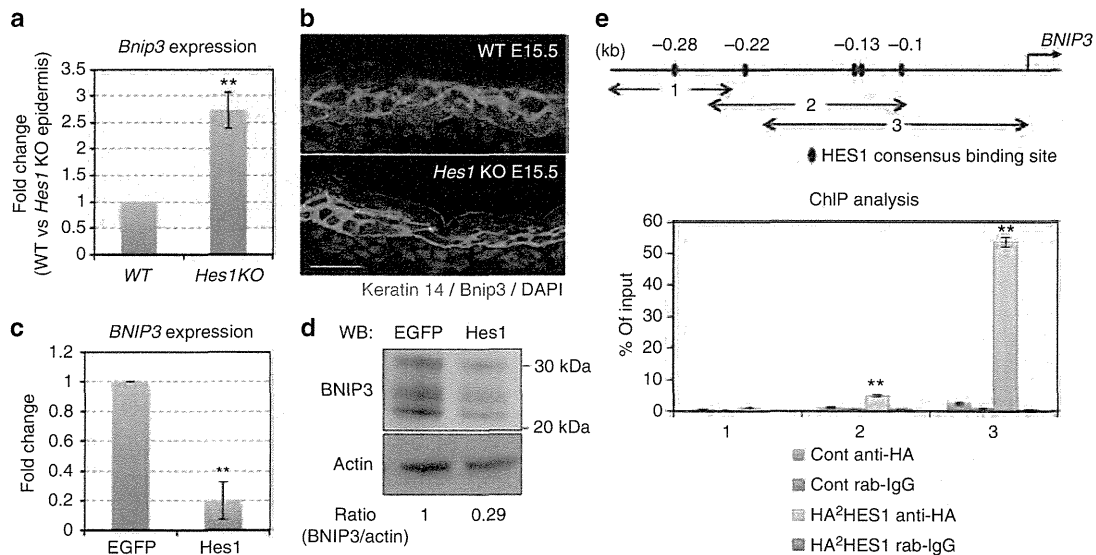
Figure 1. BNIP3 (BCL2 and adenovirus E1B 19-kDa-interacting protein 3) is directly suppressed by HES1 (hairy and enhancer of split-1). (a) Quantitative PCR (Q-PCR) analysis of *Bnip3* expression in dorsal skin epidermis from either wild-type (WT) or *Hes1* knockout (KO) embryo (embryonic day 14.5 (E14.5)). (b) Immunofluorescent analysis of Bnip3 expression in dorsal skin epidermis from either WT or *Hes1* KO embryo (E15.5). Keratin 14 staining is shown in green and Bnip3 staining is shown in red. The blue signals indicate nuclear staining. Scale bars = 20 μm. (c) Q-PCR and (d) western blot analysis of BNIP3 expression in human primary epidermal keratinocyte (HPEK) cells infected with adenoviruses expressing enhanced green fluorescent protein (EGFP) or Hes1. (c) Each expression value was calculated with the ΔΔCt method using *UBE2D2* as an internal control. (d) Numbers below blots indicate relative band intensities as determined by ImageJ software. (e) Specific binding of Hes1 to the *BNIP3* promoter. HPEK cells were infected with adenoviral constructs expressing hemagglutinin (HA)-tagged Hes1, and processed for chromatin immunoprecipitation (ChIP) with an anti-HA antibody and normal rabbit immunoglobulin G (Cont rab-IgG) as a nonimmune control. Q-PCR amplification of the region of the *BNIP3* gene described in the indicated map (upper panel; nucleotides − 360 to − 244 (1); nucleotides − 247 to − 87 (2); − 212 to + 22 (3)) was also performed. The amount of precipitated DNA was calculated relative to the total input chromatin. All the data represent the average of three independent experiments ± SD. **$P < 0.01$.

with a BNIP3 adenoviral vector. BNIP3 expression was found to be sufficient to trigger the formation of EGFP-LC3 puncta that was significantly reduced by addition of 3-methyladenine (3-MA), an inhibitor of autophagy (Figure 3a and b). On the other hand, BNIP3 knockdown markedly decreased the punctuate distribution of EGFP-LC3 in differentiated HPEKs (Figure 3c and d). Furthermore, flow cytometry analysis using a green fluorescent probe used to specifically detect autophagy (Cyto-ID autophagy detection dye) (Chan *et al.*, 2012) also showed that BNIP3 was required for the autophagy induction (Figure 3c and f). These data indicate that BNIP3 is involved in the induction of autophagy in HPEKs. Intriguingly, these data also confirm the previous finding that autophagosome induction is accompanied by keratinocyte differentiation (Haruna *et al.*, 2008). We observed that the number of mitochondria was decreased in the granular layers, where BNIP3 expression and autophagosome formation was observed (Figure 4a). In addition, mitochondria were significantly decreased in the differentiated HPEKs *in vitro* (Figure 4b). Colocalizations of mitochondria and EGFP-LC3 dot were observed only in the differentiating keratinocytes (Figure 4c), suggesting the contribution of autophagy in the decrease of mitochondria. BNIP3 expression was also correlated with decreased mitochondria in HPEKs, whereas addition of 3-MA restored mitochondrial numbers (Figure 4d). Furthermore, we also observed colocalization of mitochondria

and EGFP-LC3 dot in BNIP3-overexpressing HPEKs (Figure 4e). These data indicated that mitochondria were removed by BNIP3-induced autophagy. Next, we investigated the involvement of BNIP3 in the differentiation of epidermal keratinocytes. Western blot analysis and immunofluorescent staining revealed that BNIP3 expression increased during differentiation (Figure 5a and b). Knockdown of BNIP3 significantly suppressed keratinocyte differentiation when the cells were treated with differentiation medium (Figure 5c and d), indicating that BNIP3 is required for terminal differentiation of keratinocyte. On the other hand, forced expression of BNIP3 in HPEKs markedly stimulated loricrin expression (Figure 5e and f). To determine whether BNIP3-dependent keratinocyte differentiation was induced by autophagy, 3-MA was added to the cells transduced with BNIP3. As shown in Figure 5e and f, 3-MA notably abolished the keratinocyte differentiation induced by BNIP3, suggesting that BNIP3 is required for terminal differentiation of keratinocyte by induction of autophagy.

BNIP3 maintains epidermal keratinocytes

To further determine the roles of BNIP3 in epidermal differentiation, the human skin epidermal equivalent was reconstituted from HPEKs stably expressing a BNIP3 RNA interference (RNAi). Unfortunately, we did not observe drastic differentiation defects; however, we unexpectedly discovered
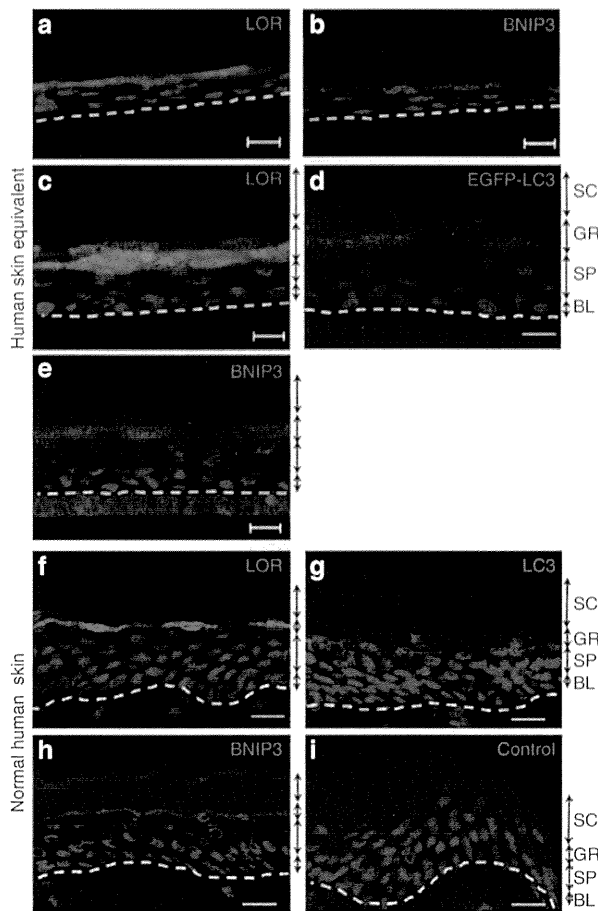
Figure 2. BNIP3 (BCL2 and adenovirus E1B 19-kDa-interacting protein 3) is expressed in the granular layer of the human epidermis. (a–e) Human skin epidermal equivalents were constituted from (a–d) normal human primary epidermal keratinocytes (HPEKs) or (e) HPEKs transfected with EGFP-LC3 by lentiviral vector. Cells were grown for (a, b) 18 days and (c–e) 24 days after exposure at the air–liquid interface. (f–i) Normal human skin epidermis. (a, c, f) Expression pattern of loricrin (LOR). (b, e, h) Expression pattern of BNIP3. (i) Control staining without BNIP3 antibody is shown. (d) Autophagosome formation determined by EGFP-LC3 puncta. (g) Endogenous expression pattern of LC3. The blue signals indicate nuclear staining. The dotted lines indicate (a–e) the boundary between the epidermis and the membrane or (f–i) the boundary between the epidermis and the dermis. Scale bars = 20 μm. BL, basal layer; GL, granular layer; SC, stratum corneum (cornified layer); SP, spinous layer.
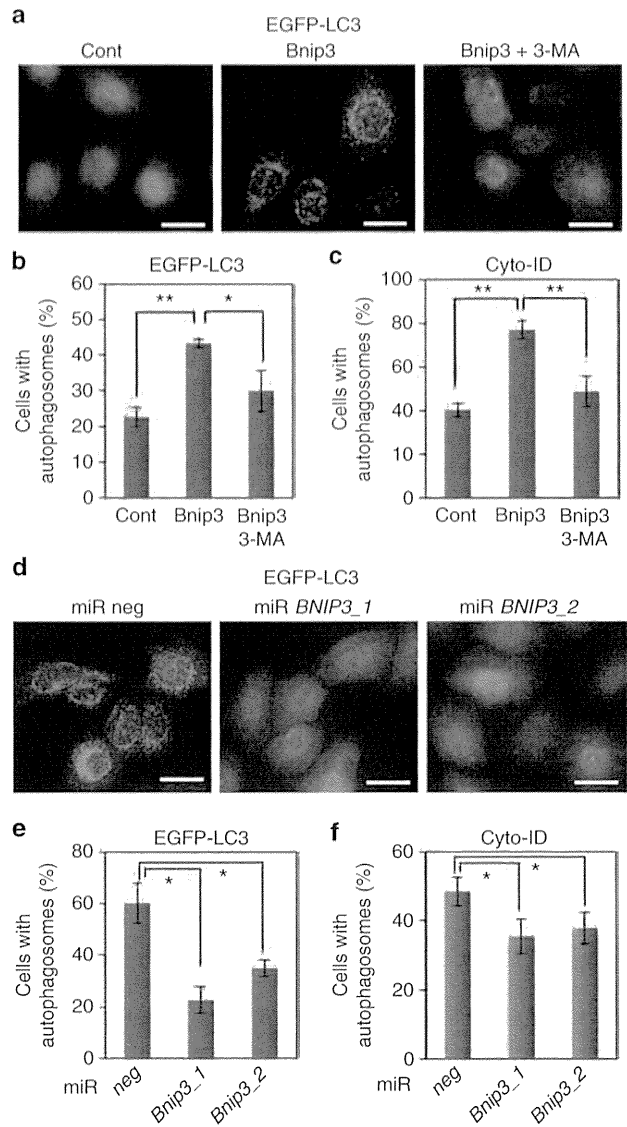

Figure 3. BNIP3 (BCL2 and adenovirus E1B 19-kDa-interacting protein 3) stimulates autophagy. (a, b) EGFP-LC3-expressing human primary epidermal keratinocytes (HPEKs) were transduced with DsRed (Cont) or BNIP3. As an inhibitor of autophagy, 3-methyladenine 3-MA (5 mM) was added. Cells were then stained with anti-EGFP at 24 hours after transduction. (a) EGFP-LC3 staining is shown in green. Scale bars = 20 μm. (b) The percentage of EGFP-LC3-positive cells with more than five puncta were quantified and are presented as the mean of three independent experiments ± SD. (c) HPEKs were transduced with DsRed (Cont) or BNIP3. As an inhibitor of autophagy, 3-MA (5 mM) was added. Autophagy induction was determined by Cyto-ID staining and quantified by flow cytometry. (d, e) EGFP-LC3-expressing HPEKs were transduced with miR neg, miR BNIP3_1, or miR BNIP3_2 and induced to differentiate. Cells were then stained with anti-EGFP at 8 hours after differentiation induction. (d) EGFP-LC3 staining is shown in green. Scale bars = 20 μm. (e) The percentage of EGFP-LC3-positive cells with more than five puncta were quantified and are presented as the mean of three independent experiments ± SD. (f) HPEKs were transduced with miR neg, miR BNIP3_1, or miR BNIP3_2 and induced to differentiate. Autophagy induction was determined by Cyto-ID staining and quantified by flow cytometry. All the data represent the average of three independent experiments ± SD. **$P < 0.01$; *$0.01 < P < 0.05$.

that "sunburn-like cells" existed in BNIP3 knockdown epidermal equivalent (Figure 6a and b). We therefore hypothesized that BNIP3 might play a key role in the survival of epidermal keratinocytes. To evaluate this hypothesis, HPEKs were irradiated with 20 mJ cm^{-2} UVB. UVB irradiation triggered the formation of autophagosome that was significantly reduced by BNIP3 knockdown (Figure 6c–e). As shown in Figure 6f, UVB irradiation induced cleavage of caspase3 and BNIP3 expression. Intriguingly, knockdown of UVB-induced BNIP3 by RNAi further increased the amount of cleaved caspase3, suggesting that BNIP3 is required for the protection of keratinocytes from UVB-induced apoptosis (Figure 6f).
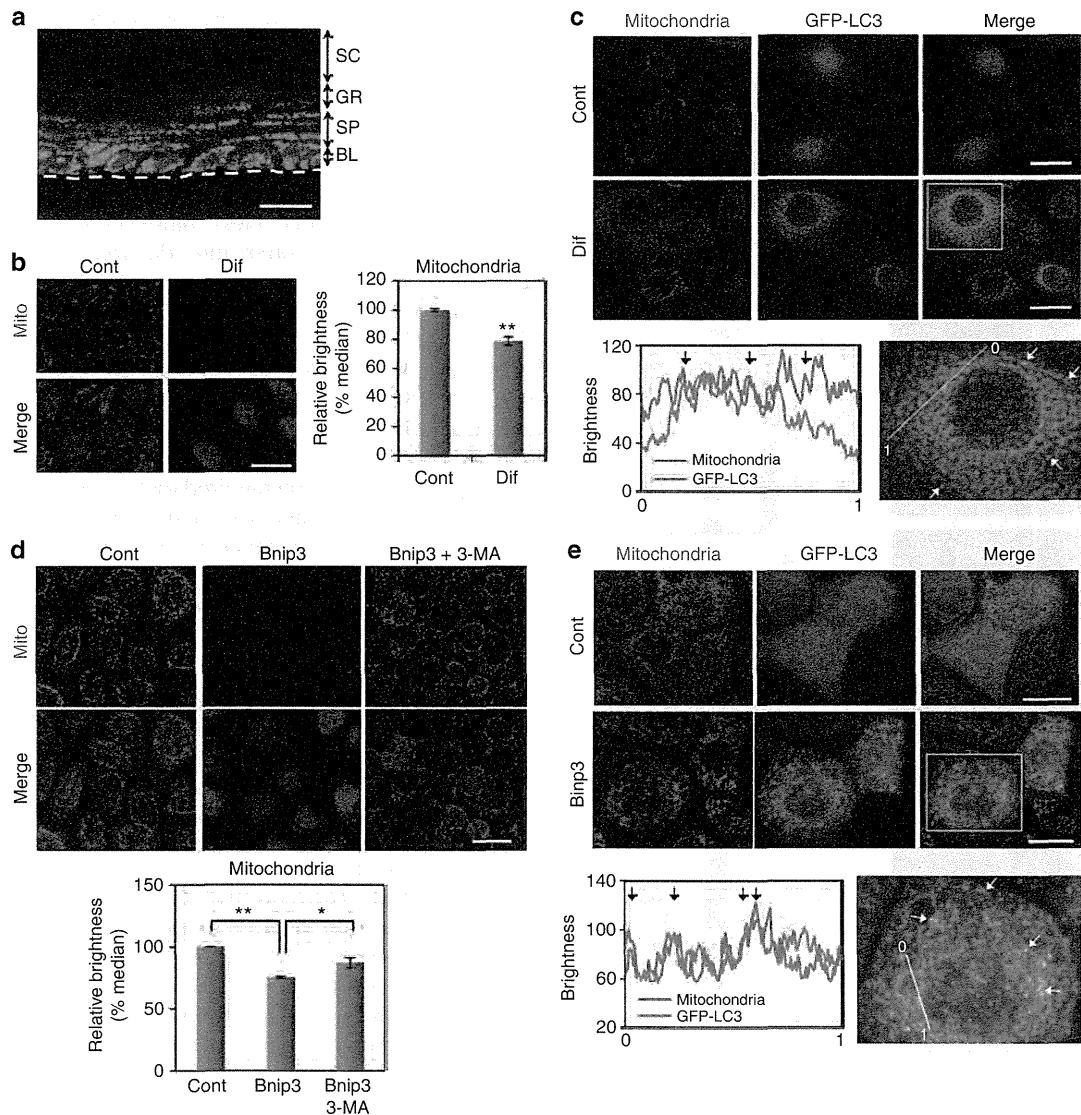
Figure 4. **Autophagy stimulates mitochondrial degradation.** (a) Distribution pattern of mitochondria. The blue signals indicate nuclear staining. The dotted lines indicate the boundary between the epidermis and the membrane. Scale bars = 20 μm. BL, basal layer; GL, granular layer; SC, stratum corneum (cornified layer); SP, spinous layer. (b) Nondifferentiated control (Cont) or differentiated human primary epidermal keratinocytes (HPEKs; Dif) were subjected to immunofluorescent staining 2 days after induction of differentiation. Mitochondrial staining is shown in red. The blue signals indicate nuclear staining. Scale bar = 20 μm. The graph indicates the percent of median brightness calculated by BZ Analyzer Software (Keyence) as the mean of three independent experiments ± SD. (c) EGFP-LC3-expressing HPEKs were differentiated. Cont or Dif were stained with anti-mitochondria (red) and anti-EGFP (green) 8 hours after induction of differentiation. Graph indicates the linescan analysis of the red and green fluorescent channels. Initial point of linescan is indicated as 0, and terminal point is indicated as 1. The arrows mark the colocalization of the two proteins. (d) HPEKs were transduced with enhanced green fluorescent protein (EGFP; Cont) or BNIP3 (BCL2 and adenovirus E1B 19-kDa-interacting protein 3). As an inhibitor of autophagy, 3-methyladenine 3-MA (5 mм) was added. Cells were then fixed and stained with anti-mitochondria 48 hours after transduction. Scale bar = 20 μm. The graph indicates the percent of median brightness calculated by BZ Analyzer Software (Keyence) as the mean of three independent experiments. **$P < 0.01$; *$0.01 < P < 0.05$. (e) EGFP-LC3-expressing HPEKs were transduced with mock (Cont) or BNIP3. Cells were then fixed and stained with anti-mitochondria (red) and anti-EGFP (green) 24 hours after transduction. Graph indicates the linescan analysis of the red and green fluorescent channels. Initial point of linescan is indicated as 0, and terminal point is indicated as 1. The arrows mark the colocalization of the two proteins.

DISCUSSION

In this study, we demonstrated that BNIP3, a potent inducer of autophagy, plays a role in the terminal differentiation and maintenance of epidermal keratinocytes. It has been suggested that autophagy plays a role in the skin epidermis, but few attempts have been made to clarify the involvement of autophagy in skin epidermis.

We found that the HES1 transcriptional repressor directly suppressed BNIP3 expression in mouse epidermis and HPEKs (Figure 1). Moreover, our results revealed that BNIP3 was
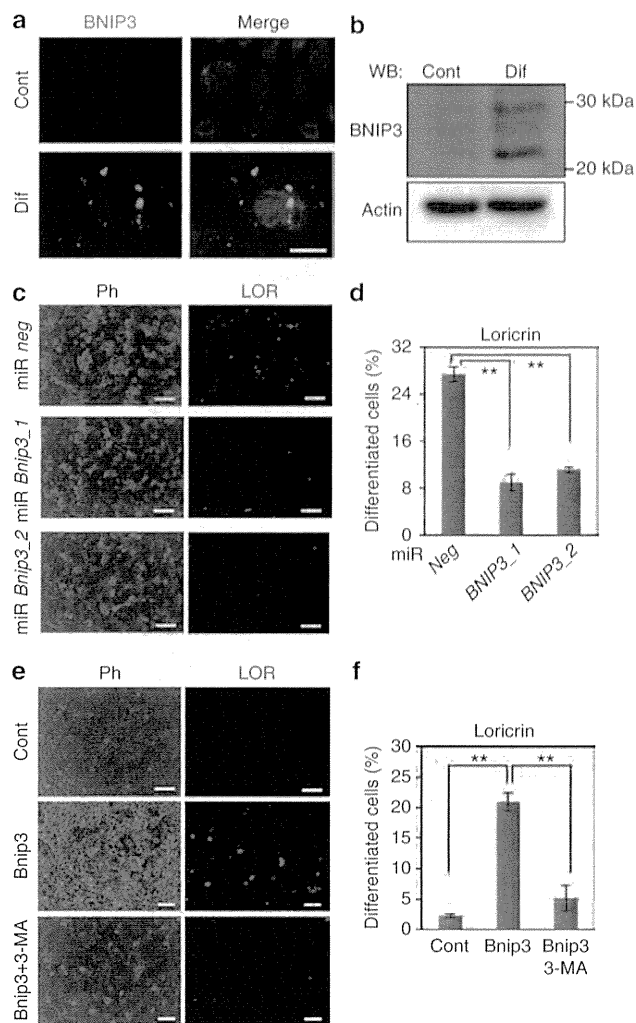
Figure 5. BNIP3 (BCL2 and adenovirus E1B 19-kDa-interacting protein 3) is required for the differentiation of keratinocytes *in vitro*. (a, b) Human primary epidermal keratinocytes (HPEKs) were differentiated and BNIP3 expression was observed. (a) Nondifferentiated control (Cont) or differentiated HPEKs (Dif) were subjected to immunofluorescent staining. BNIP3 staining is shown in green. Mitochondrial staining is shown in red. The blue signals indicate nuclear staining. Scale bar = 20 μm. (b) Western blot (WB) analysis. Proteins extracted from Cont or Dif were probed with anti-BNIP3 or anti-actin. (c, d) HPEKs were infected with adenoviral vectors expressing miR *neg*, miR *BNIP3_1*, or miR *BNIP3_2* followed by induction of differentiation. Cells were then immunostained with a loricrin antibody 9 days after transduction. (e, f) HPEKs were infected with adenoviral vectors expressing enhanced green fluorescent protein (EGFP; Cont) or BNIP3 and subjected to immunofluorescent staining against loricrin (LOR) 6 days after transduction. As an inhibitor of autophagy, 3-methyladenine 3-MA (5 mM) was added. Phase contrast images (Ph) and LOR staining are shown. Scale bars = 200 μm. (d, f) Percentages of LOR-positive differentiated cells were calculated by computerized image analysis. The data represent the average of three independent experiments ± SD. **$P<0.01$.

expressed in the granular layers of mouse epidermis, its human skin epidermal equivalent, and its normal human skin epidermis (Figures 1 and 2). These data are consistent with our

previous report showing that Hes1 is expressed in the spinous layers, where it represses the regulatory genes for differentiation to maintain the spinous cell fate (Moriyama *et al.*, 2008). Hence, it can be inferred that Bnip3 expression is suppressed in the spinous layers by Hes1, whereas it is upregulated in the granular layers where Hes1 expression is absent. In addition, our finding that BNIP3 is required for keratinocyte differentiation fits our idea that Hes1 represses certain regulatory genes to prevent the premature differentiation of spinous cells. Our *in vitro* data suggest that BNIP3 is involved in keratinocyte differentiation through autophagy (Figures 3–5). The mechanisms underlying the involvement of autophagy in keratinocyte differentiation remain elusive; however, considering that keratinocyte differentiation induced mitochondrial clearance and BNIP3 expression (Figure 4 and 5), BNIP3-induced autophagy may be responsible for the removal of mitochondria that may be required for the terminal differentiation of epidermal keratinocytes. During reticulocyte differentiation, programmed clearance of mitochondria induced by BNIP3L/Nix, a molecule closely related to BNIP3, has been reported to be a critical step (Schweers *et al.*, 2007). Therefore, keratinocytes likely possess the same differentiation mechanism that reticulocytes have, although further investigation will be required for elucidation.

In contrast to the results from differentiation in two-dimensional culture, we did not observe drastic differentiation defects in the BNIP3 knockdown human epidermal equivalent except for the existence of "sunburn-like cells" (Figure 6). This might be because of the incomplete suppression of BNIP3 in the BNIP3 knockdown keratinocytes, and/or might be because of the redundancy between BNIP3 and BNIP3L/Nix, a homolog of BNIP3, as we found in our preliminary study that Bnip3l is also expressed in the epidermis (data not shown). Although the phenotypes of BNIP3-null mice were published in 2007, these researchers found that BNIP3-null mice had no increase in mortality or apparent physical abnormalities (Diwan *et al.*, 2007). Generally, impairment of epidermal differentiation or skin barrier formation results in an obvious defect. Thus, BNIP3-null epidermis seems to exhibit subtle, if any, abnormalities. On the basis of these findings, the involvement of BNIP3 in epidermal differentiation must be investigated in the future. In-depth analysis of the BNIP3-null epidermis phenotype could help elucidate the role of BNIP3 in mouse epidermal differentiation.

Despite the lack of obvious differentiation defects in the human epidermal equivalent, our data showing that BNIP3 knockdown caused the appearance of "sunburn-like cells" is regarded as an example of apoptosis (Young, 1987), revealing a new role of BNIP3 in keratinocyte maintenance. Furthermore, requirement of BNIP3 for protection from UV-induced apoptosis was confirmed in two-dimensional keratinocyte cultures (Figure 6e). The underlying mechanism of this prosurvival function of BNIP3 in keratinocytes remains unclear; however, previous reports have demonstrated that hypoxia-induced autophagy through BNIP3 is critical for the prosurvival process (Bellot *et al.*, 2009). Recently, it has been reported that UVA induces autophagy to remove oxidized phospholipids and protein aggregates in epidermal keratino-
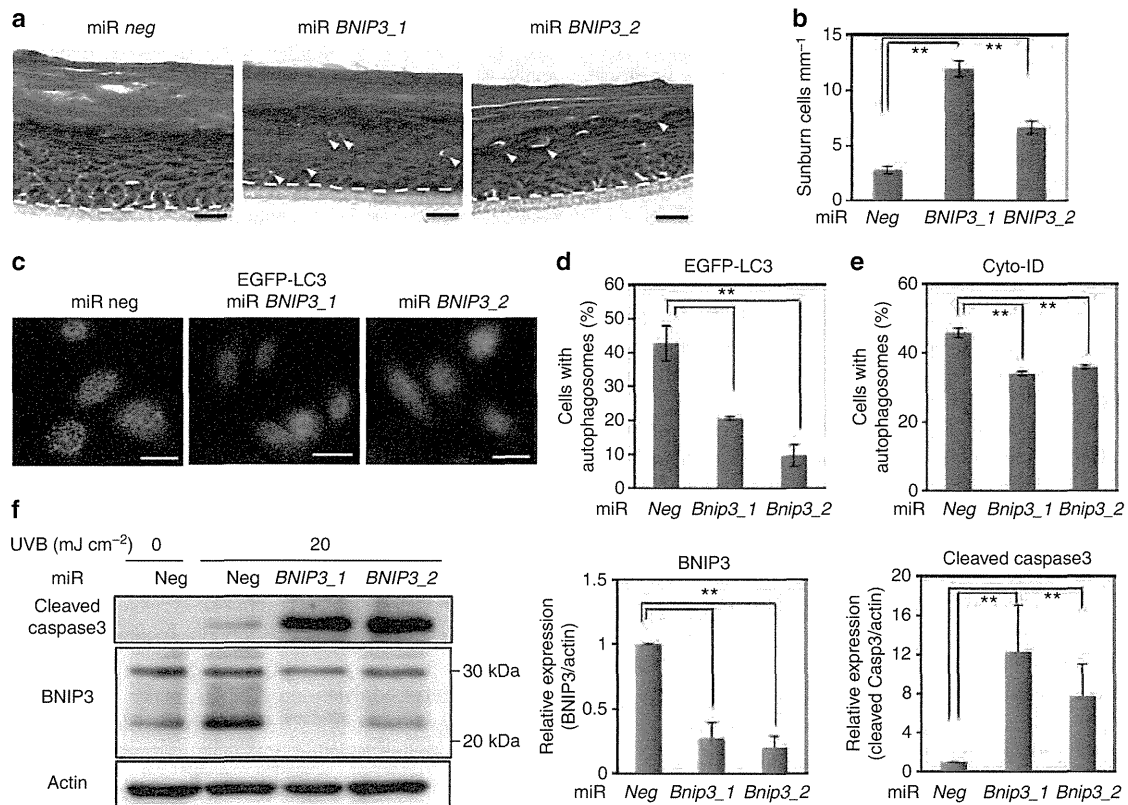
Figure 6. BNIP3 (BCL2 and adenovirus E1B 19-kDa-interacting protein 3) promotes cell survival in the reconstituted epidermis and keratinocytes.
(a) Morphology of the human skin epidermal equivalents from human primary epidermal keratinocytes (HPEKs) infected with lentivirus expressing miR *neg*, miR *BNIP3_1*, or miR *BNIP3_2*. Arrowheads indicate sunburn-like cells. (b) The number of sunburn-like cells per mm was counted and plotted as the means of 10 sections ± SD. (c–e) HPEKs were infected with adenovirus expressing miR *neg*, miR *BNIP3_1*, or miR *BNIP3_2*, and irradiated with UVB. (c) Cells were stained with anti-EGFP at 8 hours after UVB irradiation. (d) The percentage of EGFP-LC3-positive cells with more than five puncta were quantified and are presented as the mean of three independent experiments ± SD. (e) Autophagy induction was determined by Cyto-ID staining and quantified by flow cytometry. The data represent the average of three independent experiments ± SD. (f) Cells were subjected to western blot analysis at 8 hours after irradiation. The blot shown is representative image of three independent experiments. Graphs indicate relative band intensities as determined by ImageJ software and plotted as the means of three independent experiments. Scale bars = 20 μm. **$P < 0.01$.

cytes (Zhao *et al.*, 2013). Because our data indicate that UVB-induced autophagy is mediated by BNIP3 (Figure 6c and d), it is possible that autophagy induced by BNIP3 also plays a role in the maintenance of keratinocytes. Further analysis is required to confirm these results.

UV-induced apoptotic cells appear within 12 hours and are predominately located in the suprabasal differentiated keratinocyte compartment of human skin (Gilchrest *et al.*, 1981). Moreover, differentiated keratinocytes appear to be most sensitive to the UV light that induces p53-dependent apoptosis (Tron *et al.*, 1998). Tron *et al.* (1998) demonstrated that differentiated keratinocytes in p53-null mice exhibited only a small increase in apoptosis after UVB irradiation compared with the increase observed in normal control animals (Tron *et al.*, 1998). Interestingly, because p53 has been reported to directly suppress BNIP3 expression (Feng *et al.*, 2011), BNIP3 might be abundantly upregulated in suprabasal cells in p53-null animals, resulting in the resistance to UVB-induced apoptosis. Indeed, our preliminary study

showed that p53 knockdown enhanced UV-induced BNIP3 expression in HPEKs (data not shown). Therefore, BNIP3 expression in suprabasal cells appears to be important for the protection of differentiated keratinocytes from normal environmental stress such as weak UV exposure *in vivo*.

A recent report on a role for autophagy in epidermal barrier formation and function was identified in *atg7*-deficient mice (Rossiter *et al.*, 2013). The authors showed that autophagy was constitutively active in the suprabasal epidermal layers as we report in this study (Figure 2). However, in contradiction to our results, the authors concluded that autophagy was not essential for the barrier function of the skin. This may be because of the presence of an alternative Atg5/Atg7-independent autophagic pathway (Nishida *et al.*, 2009) in the epidermis. This Atg5/Atg7-independent pathway is also independent of LC3, but forms Rab9-positive double-membrane vesicles. Moreover, protein degradation via this pathway is inhibited by 3-MA and is dependent on Beclin 1. Our data demonstrate that: (1) BNIP3 induced the formation of

EGFP-LC3 puncta (Figure 4) and (2) 3-MA significantly diminished the formation of GFP-LC3 puncta and keratinocyte differentiation induced by BNIP3 (Figure 5). These findings suggest that BNIP3 in the epidermis induced both conventional and Atg5/Atg7-independent autophagy. Intriguingly, GFP cleaved from GFP-LC3 also accumulates in the *Atg7*-deficient epidermis (Rossiter *et al.*, 2013), thereby demonstrating the existence of an alternative autophagic pathway (Juenemann and Reits, 2012) in the epidermis. Further investigation will be required to determine whether Beclin 1 and Rab9 are indispensable for the BNIP3-induced autophagy and subsequent differentiation of keratinocytes.

In summary, our data reveal that expression of BNIP3 in granular cells induces autophagy and is involved in the terminal differentiation and maintenance of skin epidermis. Studies on the involvement of autophagy in skin epidermis have attracted considerable attention recently. In addition, increasing evidence suggests the involvement of BNIP3 in the differentiation of several cell types, including oligodendrocytes (Itoh *et al.*, 2003), osteoclasts (Knowles and Athanasou, 2008), and chondrocytes (Zhao *et al.*, 2012); however, the precise role of BNIP3 in this process remains to be investigated. Our study thus provides new insights into the functions of BNIP3 in differentiation and homeostasis.

MATERIALS AND METHODS

Histology and immunofluorescent analysis
Samples and embryos were fixed in 4% paraformaldehyde, embedded in optimal cutting temperature compound, frozen, and sectioned at 10 μm. Sections were then either subjected to hematoxylin and eosin staining or immunohistochemical analysis as previously described (Moriyama *et al.*, 2006). Details are described in Supplementary Materials Online.

Cell culture
HPEKs were purchased from CELLnTEC (Bern, Switzerland) and maintained in CnT-57 (CELLnTEC) culture medium according to the manufacturer's protocol. For induction of differentiation, the medium was changed to CnT-02 (CELLnTEC) at confluent monolayers of HPEKs, followed by adding calcium ions to 1.8 mM. The generation of human skin equivalents was performed using CnT-02-3DP culture medium (CELLnTEC) according to the manufacturer's protocol.

Design of artificial microRNAs and plasmid construction
Oligonucleotides targeting a human BNIP3 sequence compatible for use in cloning into BLOCK-iT Pol II miR RNAi expression vectors (Invitrogen, Carlsbad, CA) were obtained using the online tool BLOCK-iT RNAi Designer. The oligonucleotide sequences used in this study are shown in Supplementary Table S1 online. Cloning procedures were performed following the manufacturer's instructions.

Adenovirus and lentivirus infection
Adenoviruses expressing EGFP, Hes1, BNIP3, and miR *BNIP3* were constructed using the ViraPower adenoviral expression system (Invitrogen) according to the manufacturer's protocol. Lentivirus expressing EGFP-LC3 (from Addgene plasmid 21073, Cambridge, MA) and miR *BNIP3* plasmid was constructed and used to infect keratinocytes as previously described (Moriyama *et al.*, 2012; Moriyama *et al.*, 2013).

RNA extraction, complementary DNA generation, and Q-PCR
Total RNA extraction, complementary DNA generation, and Q-PCR analyses were carried out as previously described (Moriyama *et al.*, 2012). Details of the primers used in these experiments are shown in Supplementary Table S2 online.

Western blot analysis
Western blot analysis was performed as previously described (Moriyama *et al.*, 2012; Moriyama *et al.*, 2013). Details are described in Supplementary Materials Online.

ChIP assay
The ChIP assay was performed using the SimpleChIP Enzymatic Chromatin IP Kit (Magnetic Beads) (Cell Signaling Technology, Danvers, MA) according to the manufacturer's instructions. Hemagglutinin-tagged Hes1 was immunoprecipitated with rabbit polyclonal antibody against hemagglutinin tag (ab9110, Abcam, Cambridge, MA). Immunoprecipitated DNA was analyzed by Q-PCR. Relative quantification using a standard curve method was performed, and the occupancy level for a specific fragment was defined as the ratio of immunoprecipitated DNA over input DNA. Details of the primers used in these experiments are shown in Supplementary Table S2 online.

Flow cytometry analysis
For autophagy detection, Cyto-ID Autophagy detection kit (Enzo Life Sciences, Plymouth Meeting, PA) was used according to the manufacturer's instructions. Details are described in Supplementary Materials Online.

SUPPLEMENTARY MATERIAL
Supplementary material is linked to the online version of the paper at http://www.nature.com/jid

REFERENCES

Aymard E, Barruche V, Naves T *et al.* (2011) Autophagy in human keratinocytes: an early step of the differentiation? *Exp Dermatol* 20:263–8

Bellot G, Garcia-Medina R, Gounon P *et al.* (2009) Hypoxia-induced autophagy is mediated through hypoxia-inducible factor induction of BNIP3 and BNIP3L via their BH3 domains. *Mol Cell Biol* 29:2570–81

Blanpain C, Lowry WE, Pasolli HA *et al.* (2006) Canonical notch signaling functions as a commitment switch in the epidermal lineage. *Genes Dev* 20:3022–35

Chan LL, Shen D, Wilkinson AR *et al.* (2012) A novel image-based cytometry method for autophagy detection in living cells. *Autophagy* 8:1371–82

Chatterjea SM, Resing KA, Old W *et al.* (2011) Optimization of filaggrin expression and processing in cultured rat keratinocytes. *J Dermatol Sci* 61:51–9